WIDE-BAND CHANNEL MODEL FOR UNDERWATER ACOUSTIC COMMUNICATION AND ITS APPLICATION TO KALMAN FILTER BASED CHANNEL ESTIMATOR

by

Apurva Deota

Submitted in partial fulfillment of the requirements
for the degree of Master of Applied Science

at

Dalhousie University
Halifax, Nova Scotia
March 2020

Table of Contents

List of Tables

List of Figures

Abstract

Underwater acoustics communication system design is a challenging endeavour due to several technical as well as environmental parameters such as salinity of water, temperature, frequency and time selectivity of the channel, different sea bed surfaces, Doppler effect and more. The task of a channel model is to provide a software that determines the channel behavior without a need for practical deployment.

In this thesis, unlike the already existing narrow-band communication channel models, a model is designed to take into account variation of the channel impulse response as a function of communication signal frequency. The proposed model utilizes a conceptually simple sum-of-sinusoids approach and incorporates frequency-dependency into the model output and is suitable for modelling multiple-input multiple-output (MIMO) channels. The model addresses multi-path fading effect and the effect of Doppler shift dependence on the signal angles of arrival.

The capabilities of the proposed model are tested by comparing with data observed during sea-trials. In addition, an OFDM based underwater transmission systems with iterative data decoding and channel estimation is used on a narrow-band and the proposed wide-band model. It is demonstrated that auto-regression channel models used to operate channel estimators need to be adjusted to address frequency dependence showcased by the wide-band channel model.

List of Abbreviations Used

EM Electromagnetic

MIMO Multiple Input Multiple Output

SIMO Single Input Multiple Output

SSP Sound Speed Profile

RMS Root Mean Square

PDF Probability Density Function

CDF Cumulative Distribution Function

OFDM Orthogonal Frequency Division Multiplexing

RC Raised Cosine

FDM Frequency Division Multiplexing

iDFT inverse Discrete Fourier Transform

AWGN Additive White Gaussian Noise

CP Cyclic Prefix

LDPC Low Density Parity Check-code

QPSK Quadrature Phase Shift Keying

LLR Log-Likelyhood Ratios

SOS Sum Of Sinusoids

PDP Power Delay Profile

MSE Mean Square Error

RE Residual Error

BER Bit Error Rate

SNR Signal to Noise Ratio

Acknowledgements

I wish to express my sincere gratitude to my supervisor, Dr. Dmitry Trukhachev, who responsibly guided and encouraged me to be consistent even when the road got tough. Without his constant help and his faith in my work, the goal of this project would not have been realised. I pay my special regards to my co-supervisor, Dr. Kamal ElSankary for his appreciable support that made this thesis a lot smoother. It would not have been possible to complete this thesis without their valuable suggestions.

I would like to thank Dr. Jason Gu and Dr. Qiang Ye to be a part of my supervisor committee and for reviewing my thesis.

I would like to recognize the invaluable technical support provided by my team member Murwan Bashir. I also wish to show my gratitude to the department of Electrical and Computer Engineering, specially to the secretaries Nicole Smith and Tamara Cantrill to process all the documentation.

I wish to express my deepest gratitude to my family: my father Dr. Bhushan Deota, my mother Jyoti Deota and my sister Asmita Deota for their undying support, encouragement and understanding throughout my graduate studies. Lastly, I thank all my friends to be there for me during this journey.

Chapter 1

Introduction

Communication underwater differs broadly from typical wireless communication with air as its medium. The main distinction can be done on the basis of types of waves used for transmission. For wireless in air communication electromagnetic (EM) waves are used, whereas, for underwater communication acoustic waves are used. This is due to the conductivity and electrically polarized nature of water which in turn reduces the range of transmission of EM waves causing higher attenuation underwater. Although sound waves carry information to longer distances than EM waves, still underwater communication remains a complex field to work with due to factors like elevated Doppler spread, varying environmental conditions, prolonged impulse response, limited frequency selection and multi-path propagation. This makes high-end system designs necessary to have a satisfactory output.

Channel model is a tool designed to help predict the output of the channel in such harsh communication environment before practically testing it underwater. Data or parameters of the channel are entered in the model and it determines if communication can be established with these parameters and the quality of response for the underwater system. For this purpose many criterion are used while designing a channel model to give the output that best matches with the real life channel behaviour. The narrow-band SOS model, is a channel model that performs the task mentioned above. However, assumptions made in narrow-band model implies that for every frequency in the given bandwidth the Doppler spread remains the same, which produces a channel that has a noticeable difference when compared to real life channel. Moreover, it does not take into consideration the Doppler shifts in the channel, further making it less productive.

This literature concentrates on modeling a channel by taking this frequency dependent nature of Doppler spread into consideration. Further, adding a feature of Doppler shifts specific to angle of arrival of each path and studying the remarkable differences that these two parameters would induce, making the model more practical, realistic and reliable.

1.1 Motivation

Encouraged by increased development and application of underwater acoustic communication various channel models are designed with different approaches till date. Even though there exists no standardized model for underwater sound communication, various models have been created and used over time focusing on different parameters while modeling. For an instance, the ray tracing model developed in [2] focuses on modeling the known time-series for two cases, that is, for steadily moving transmitter or receiver and considering wave motion in its second case. This approach makes the ray tracing model more effective and faster in comparison to previous ray tracing models that were confined to a narrower approach as discussed in [2]. Whereas, PECan model illustrated in [3] proceeds using a parabolic equation for underwater sound propagation. Moreover, a statistical method is adopted in [4] constructing a point-to-point model. This model takes into consideration the channel dynamics depending on physical processes occurring during underwater acoustics propagation, focusing on small scale effects like scattering and Doppler shifts and large scale effects like locally received average power, environmental conditions and location uncertainty. One of the model given in [5] concentrates on the modeling of the QD (Quadrature Detector) response in the presence of rough boundaries, reserving inclusion of effects caused by a time-varying sea surface or source/receiver motion to future implementations. Where as, research done in [6] determines the impact of receiving depth, sea bottom boundary, and sea surface boundary on channel estimation.

There have been several attempts to construct a MIMO (Multiple Input Multiple Output) channel model. The MIMO channel models are approached either by upgrading the point-to-point model and including array geometry for multiple transmitter and hydrophones as given in [7], or by actually introducing transmitter and receiver correlation as presented in [8]. Further, the model in [9] focuses on creating artificial test channels that generates communication algorithms with similar challenges as faced in channels during sea trials. This model is less complex and also considers hydrophone correlation making it SIMO (Single Input Multiple Output) model. Statistical model artificially generating channel tap variations is also discussed in [10], where path dynamics are obtained using random Gaussian process and Doppler spectrum measured during sea trials. Also, [11] briefs one such model. However, these channel models are point-to-point models and we have no control over fading from dynamics that can be obtained from model in [9]. Though the model in [9] is a SIMO model and uses SOS (Sum of Sinusoids) technique, it cannot account for frequency specific Doppler effects (Doppler shifts and Doppler spreads), which are observed to be critically important parameters while running the real life channels with the same model. Moreover, all the models stated here are insensitive to path and frequency specific Doppler shifts.

The channel model proposed in this study is an upgrade for model in [9] that is also SIMO and is known as wide-band channel model. This is because, wide-band channel model generates frequency specific Doppler spreads for more accurate and relevant results. Also, as it is frequency dependent it provides reliable results not only for small bandwidths but also for higher bandwidths. Furthermore, this project adds a feature of Doppler shifts respective to arrival angle of each path which is complex to compensate and hence, necessary to be added as an effect on channel. Implementation of this model provides a tool that can be used confidently for underwater systems to examine the output quality of the setup.

1.2 The Outline

This thesis is organized as follows:

1. Chapter 2 reviews some background theories, concepts and setups used in this project.

2. Chapter 3 demonstrates theoretical and mathematical representation for the channel and OFDM on the derived channel for frequency dependent (wide-band) channel model.

3. Chapter 4 comprises of detailed implementation approach of channel in MATLAB, transmission and estimation system in Simulink and additional Doppler shift feature of this model.

4. Chapter 5 illustrates the results when this setup is used for various underwater systems with a brief discussion on each experiment, results of sea-trials and brief on making Auto-regression model a wide-band model.

5. Chapter 6 concludes the thesis and proposes some potential future work.

Chapter 2

Background Study

This section introduces terms, concepts and theories that are pillars of this project. Some theories are basics of wireless communication, while some of them are specific for underwater communication done with the help of sound waves.

2.1 Multi-path Propagation

Transmission environment of water bodies like oceans can be imagined as a structure with rough moving top surface and a non-mobile rough bottom surface. While transmitting acoustic signal, reflections take place on the top surface as well as bottom surface and often on both the surfaces creating multiple reflection pattern depending on the surface waves and type of the ocean bed. Moreover, the sound speed varies as the signal travels in different water columns, undergoing one or several refraction. These phenomenons result in several paths of signal that hit the transmitter with different delays. These paths are referred as ”path-bundles” [1] or ”echoes” [4]. The delays caused between path-bundles generates a stretched impulse response of the input signal. Often some paths that arrive with very short delays are considered as one path justifying the name path-bundles. Figure 2.1 depicts a power delay profile of a signal gone through underwater multi-path propagation.

2.2 Sound Speed Profile

Sound Speed Profile (SSP) is the data accumulated for speed of sound at different depths of water. It is generally seen in a tabular form or in a plot like Figure 2.2. Sound speed not only depends on the the depth, but also depends on temperature and salinity of the water at

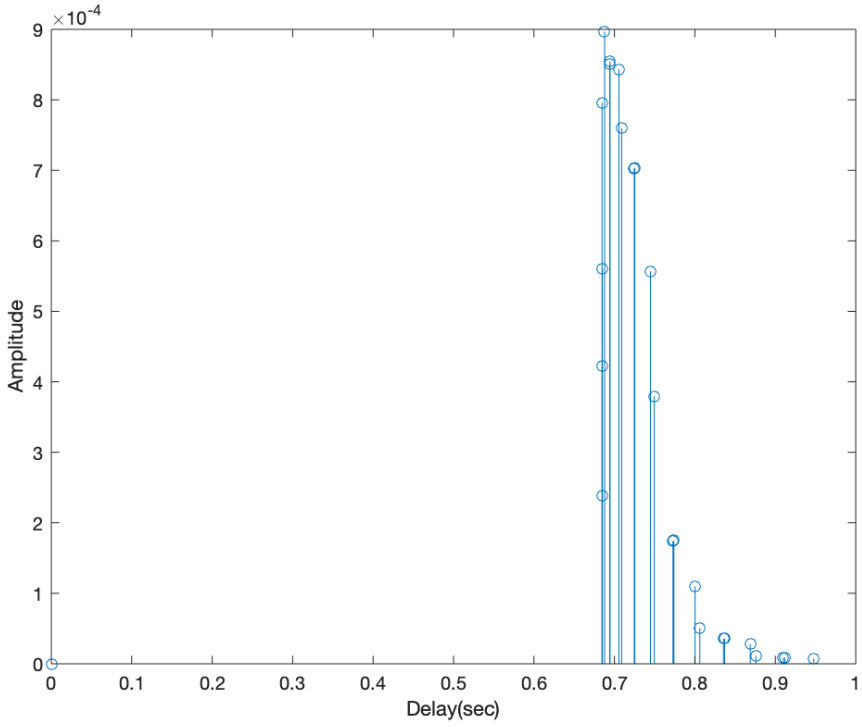

Figure 2.1: Multi-paths or Taps in Amplitude-Delay profile

different levels in the water body. Hence, SSP for every water body varies and is measured during ocean experiments. SSP plays a crucial role while using bellhop to trace the rays, predict the path of arrival rays, quality of signal, etc.

2.3 Surface Scattering

An underwater system in the live environment like sea or ocean has a fixed rough bottom surface, but has a continuously varying top surface with variable roughness. This mainly depends on the wind speed of the location as it affects wave breaking and wave movement. This environmental factor has significant effect on scattering of signal waves. Moreover, air bubbles at the sea surface are also responsible for scattering of the transmitted signal. For a rough weather day, when the sea surface is highly irregular and when the signal transmitted hits the rough top surface, the signal reflected back is scattered forming more multi-paths.

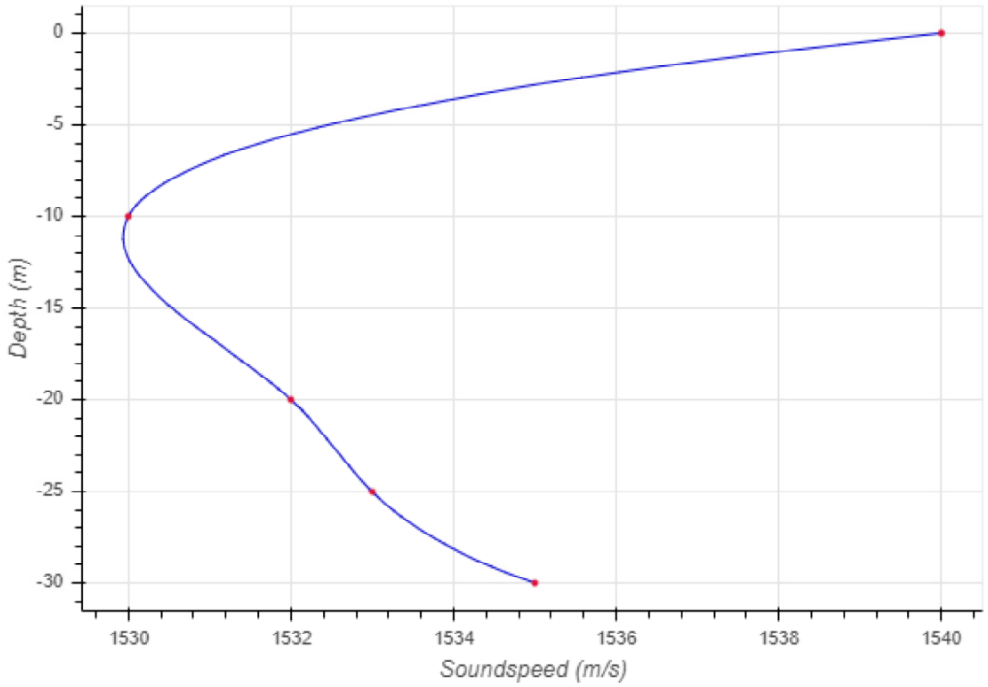

Figure 2.2: Example Figure for Sound Speed Profile

This happens every time a path undergoes top surface bounces, resulting in a signal that has different arrival delays, and angles for each path. As, the wave surface is changing with time, the signal arrivals at receiver are not localized as in the case of calm weather. That is, instead of forming path bundles they arrive as scattered signal with larger delays and forming a harshly time varying impulse response. While, in the case of calm weather the wave motion is softer and thus, scattering is comparatively less and the signal is localized or bunched to give a better output. The most noticeable effect of this top surface scattering is on Doppler spread, as the spread increases with the increase in roughness of the surface. [1]

2.4 Doppler Shifts

Doppler shifts take place due to intentional or unintentional movement of transmitter or receiver. This motion induces frequency shifts in each path of the signal. These frequency

shifts are given by the following formula, [12] [13]

$$\Delta f = f_0 \frac{V}{c} \text{Hz} \tag{2.1}$$

Where, V is the velocity of moving transmitter, c is the speed of sound in water (Considered to be 1500 m/s for a practical underwater system.), f_0 is the actual frequency. It can also be given as,

$$\Delta f = V \cos \theta_i \tag{2.2}$$

Here, θ_i is the angle of arrival for each path. Hence, it can be deduced from this equation that this effect is path specific. Figure 2.3 depicts this phenomenon.

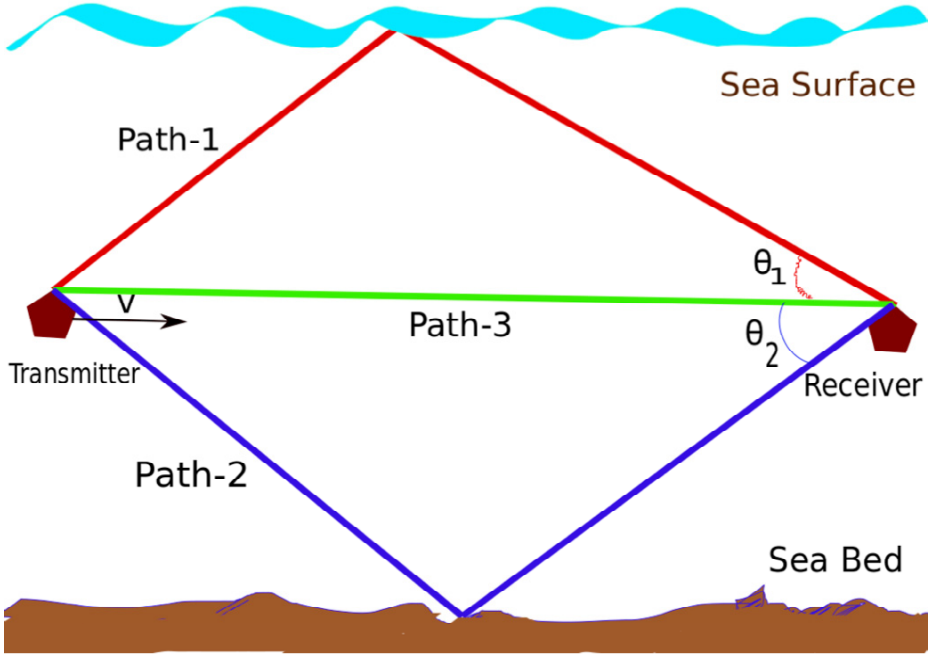

Figure 2.3: Multi-path Propagation in Underwater Environment

2.5 Doppler Spread

In multi-path propagation the phase-shifted signals arriving from different directions cause fading due to destructive interference. Moreover, this multi-path propagation also creates a

scenario where Doppler shifts of different paths are different. This frequency-shift between two signals also results into fading. The difference between Doppler shifts of two signal paths transmitted from same source but traveling with different paths is known as Doppler spread. This spread increases with number of bounces the signal wave undergoes from the top ocean surface [9]. For an example, Doppler frequency of path-1 in figure 2.3 will be different than that of path-2, which will cause Doppler spread and a fading effect. Now, as seen in expression 2.1 the Doppler shift is frequency dependent, which suggests that at higher frequency the Doppler-shift-frequencies are higher. Further, as discussed in [14] Doppler spread and Doppler shifts highly depend on frequency and velocity of moving transmitter or receiver. This fact is one of the base for this project.

2.6 Narrow-Band Model based on Sum-of-Sinusoids (SOS)

A channel model is an implementation that forecasts the performance of a underwater system before its actual use and thus is a great help for designing an underwater system. For the purpose of modeling frequency dependent model (Wide-Band Model), it is important to understand the frequency independent model (Narrow-Band Model). The narrow-band/ Frequency Independent channel model principles are presented in the literature [4] which are broadly discussed in [1] and [9].

This model is based on sum of sinusoids and is illustrated in the block diagram 2.4, where the inputs to the channel are power-delay profile, Doppler spread profile and other system parameters. The power-delay profile is derived from the data produced by bellhop's arrival file, which takes the input parameters like depth of transmitter, depth of receiver, transmission distance, sound speed profile measured in same ocean environment during practical experiments and provides a data file consisting of arrival angle, delays, amplitude and more.

With reference to [9], considering we have p number of paths, for $l = 1, 2..p$, in the

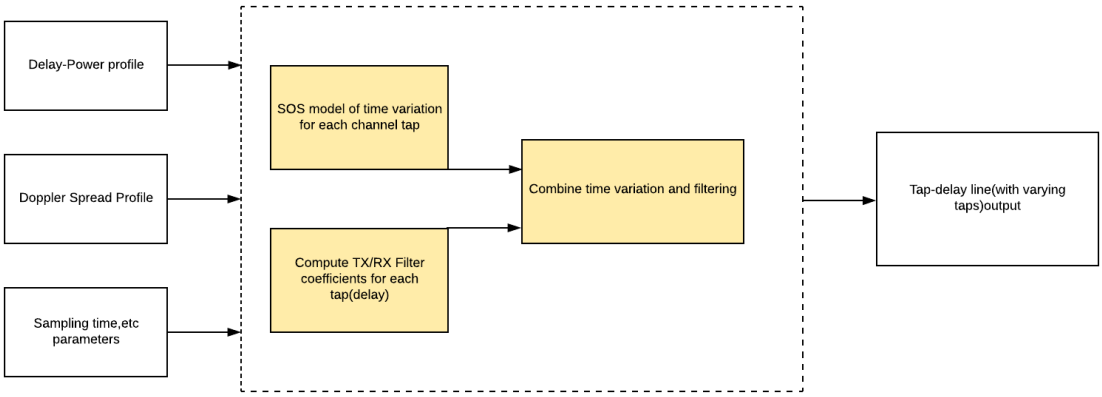

Figure 2.4: SOS Model Block Diagram [1]

least complex scenario, a Doppler spread function $S_l(v)$ assigned for every path can be considered as Root Mean Square(RMS) Doppler spread of all the paths and is symbolised as α_l. The Doppler spread function is represented as exponentially decaying probability density function (PDF) [15],

$$S_l(v) = \frac{1}{2\alpha} e^{-\frac{|v|}{\alpha}} \tag{2.3}$$

To generate samples, inverse transform sampling lemma is used, which is a mathematical method of generating random numbers from any probability distribution by using inverse cumulative distribution function (CDF) $F^{-}(y)$. Cumulative Distribution of random variable X is distributed uniformly over [0,1] if X is chosen according to $f(x)$. Hence, here taking y uniformly distributed over [0,1] we can obtain X (samples) according to $f(x)$ using inverse cumulative Distribution function.

This can be simply represented as $X = F^{-}(y)$ [1]. Utilizing 2.3,

$$F(f_m) = \int_{-\infty}^{f_m} \frac{1}{2\alpha} e^{-\frac{|v|}{\alpha}} \, \mathrm{d}v = \frac{\mathrm{sng}(f_m)}{2}(1 - e^{-|f_m|/\alpha}) \tag{2.4}$$

With the help of inverse transform sampling and setting $F(f_m) = u$, where u is uniformly distributed over [0,1], we generate f_m with PDF of $S_l(v)$. This can be mathematically

portrayed as,

$$f_m = -\alpha \log(\mathrm{mod}(2u, 1))\mathrm{sgn}(1 - 2u) \tag{2.5}$$

The final input block in Figure 3.1 represents other input parameters such as sampling time, bandwidth, carrier frequency and so on.

In discourse of time variation block using SOS model, the channel impulse response using sum-of-sinusoids can be attained in the form of time samples that can be represented as,

$$h[i]_{Rayleigh} = \frac{1}{\sqrt{M}} \sum_{m=1}^{M} e^{j(\phi_m + 2\pi f_m i T_s)} \tag{2.6}$$

Where $h[i]$ are discrete time samples, T_s is sampling time which represents t as iT_s, M are the total number of sinusoids the model uses to represent time variation of the taps, f_m are the Doppler frequencies that are utilized for Doppler spectrum of channel tap , generated using equation 2.5 and are also as many as M, ϕ_m are the initial phases of sinusoids which are random and distributed over a uniform interval of $0\ to\ 2\pi$. As M increases the amplitude tends to become more accurately Rayleigh distributed. However, 500 sinusoids are considered in experiments presented in chapter 5 that provides justifiable results.

In order to study filtering block we consider the methodology in [16] which is also considered in [1]. According to the same, the channel impulse response of a frequency selective channel is given by,

$$h(t; \mathcal{T}) = \sum_{p=1}^{P} C_p(t)\delta(\mathcal{T} - \mathcal{T}_p) \tag{2.7}$$

This equation depicts a channel with P multi-paths, where each path indeed is a path-bundle. This fact results in fading behaviour of $C_p(t)$. Moreover, as given in [1] the

Doppler spectrum of $C_p(t)$ cannot be considered same as it is considered for radio communication channel because for underwater acoustic communication this approach is inappropriate as Doppler spectra are not only delay specific but are more stretched for higher frequencies of bandwidth than lower frequencies. They are caused by wave movements on the surface of water body and the paths with multiple surface bounces have broader Doppler spectrum. However, frequency dependency of Doppler spectrum is not considered in this model but is considered in Wide-band model. The model in expression 2.7 is infinite band, so it cannot be directly implemented for a system where filtering at Transmitter and Receiver is to be taken into account. Figure 2.5. shows one such system. Here, x_i are the

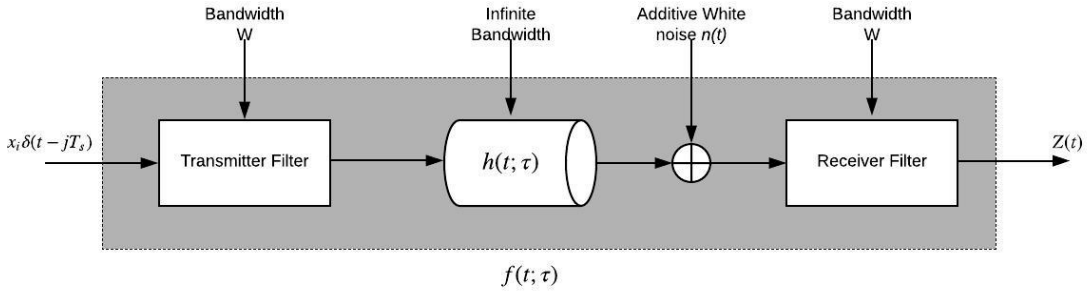

Figure 2.5: Filter model of a multipath fading channel [1]

complex transmit samples that pass through a transmit filter with an impulse response of g(t). Further, it passes through the channel and finally through a receive filter to give the output signal $z(t)$. The signal $z(t)$ is then sampled using symbol time T or T_s (Symbol time used instead of T for less complex calculations.) The system formed here is discrete linear time-varying filter which can be mathematically expressed as,

$$f(t;\mathcal{T}) = h(t;\mathcal{T}) * g(\mathcal{T}) * g(-\mathcal{T}) = h(t;\mathcal{T}) * g_{\text{total}} \tag{2.8}$$

The output $z(t)$ can be given as,

$$z(t) = f(t;\tau) * x_i(t) + n(t) \tag{2.9}$$

For discrete sample model $Z(kT_s) = Z_k$

$$Z(kT_s) = \sum_{j=k}^{k+L-1} x_j f(kT_s, (k-j)T_s) + n_k \tag{2.10}$$

$$= \sum_{l=1}^{L} x_{k-l} f(kT_s, lT_s) + n_k$$

$$= \sum_{l=1}^{L} x_{k-l} f_l(KT_s) + n_k$$

The equation 2.10 gives a tap delay line model of a channel with time varying ISI (inter-symbol interference). Pictorial representation of this model is in Figure 2.6 .

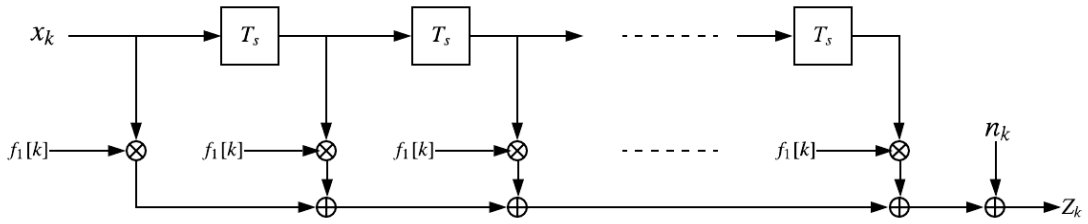

Figure 2.6: Tapped delay-line model of the same multi-path fading channel. [1]

In order to calculate Z_k we need to generate the values of time varying taps, that is to generate values for $f_l[k]$. For this purpose the equation of time samples of impulse response (equation 2.6) is to be associated with equation 2.8. Hence $f_l[k]$ can be generated by,

$$f_l[k]_{Rayleigh} = \frac{1}{\sqrt{M}} \sum_{m=1}^{M} e^{j(\phi_m + 2\pi f_m(kT_s - \tau_m))} * g_{\text{total}}(lT_s - \tau) \tag{2.11}$$

In this case the channel is considered single tap with average unit power and τ as its delay. To keep this formula generic there is no further simplification for $g(\tau)$ except mentioning it as a low pass filter with bandwidth W and sample time $T_s = \frac{1}{2W}$. The above channel model and the frequency dependent model (discussed in next section) both uses raised

cosine (RC) pulses with a roll off factor.

2.7 OFDM over doubly spread channels

OFDM is an advancement in FDM (Frequency Division Multiplexing), extensively used in new generation wireless communication. This multiplexing technique is frequency division multiplexing but with closely spaced sub-carriers, without any guard bands between them. Most-importantly, these sub-carriers are orthogonal to each other . This method enables the user to send more data over same bandwidth. Though, in frequency domain sub-carriers overlap each other but, the orthogonal arrangement of these carriers prevents interference. The orthogonality of sub-carries implies that at a peak of one data signal other signals are at zero, making it possible for a demultiplexer to separate these independent signals. Along with high transmission rate, OFDM technique has other advantages like, it does not require high-end band-pass filter for separation of carriers as required in FDM [1]. Moreover, its modulation and demodulation is less complex using Fast Fourier Transform (FFT) as explained in [17]. While, OFDM holds so many advantages, it is sensitive to cross-talk in unwanted time variation scenario. Also, high peak-to-average power ratio is its another significant disadvantage. However, improvements in linear amplifiers' technology have nullified this disadvantage [18]. This setup utilizes Class D amplifiers. This section goes into detail structure of OFDM as given in [18] and [1].

For a baseband signal as described in [1], the channel bandwidth W is divided into N (complex sub-carriers). The frequencies here are spaced at a distance of Δf , that is given as,

$$\Delta f = f_{k+1} - f_k \tag{2.12}$$

Where, f_k stands for k frequencies and k=[0,N-1]. f_k can be given as.

$$f_k = k(W/N) \tag{2.13}$$

The rate at which symbols are transmitted is given by inverse of symbol duration. For symbol time T,

$$r = 1/T = \Delta f = W/N \tag{2.14}$$

If T_s is symbol time for single carrier, $W = 1/T_s$. Therefore, $T = NT_S = N/W$ and $f_k = k/T$. Now, as the two waveforms are orthogonal to each other their inner product will be null. This can be represented as,

$$\int_0^T e^{2\pi f_i t} e^{2\pi f_j t} dt = 0, \tag{2.15}$$

This holds true for every $i \neq j$. Advantage of orthogonality is that the rate of sending data that can be decoded independently increases from $r_s = 1/T_s = N/T$ to $r = r_s/N$ by parallel transmission of N symbols utilizing same bandwidth W. The baseband signal transmitted at output of an analog OFDM being complex in nature is given by,

$$x(t) = \sum_{k=0}^{N-1} X[k] e^{j2\pi f_k t} \tag{2.16}$$

$$= \sum_{k=0}^{N-1} X[k] e^{j2\pi kt/T}, \quad 0 \leq t < T$$

Here, $X[k]$ is the constellation point at kth position and at times $t \to nT_s$ if $x(t)$ is sampled discrete samples are generated as below.

$$x[n] = \sum_{k=0}^{N-1} X[k] e^{j2\pi k(W/N)nT_s} \tag{2.17}$$

Considering the fact $T_s = 1/W$, $x[n]$ becomes complex baseband time sequence,

$$x[n] = \sum_{k=0}^{N-1} X[k] e^{j2\pi kn/N}, \quad 0 < n \leq T \tag{2.18}$$

As depicted in above equation, $x[n]$ is inverse Direct Fourier Transform (iDFT) of $X[k]$(that is $x[n] = iDFT\{X[k]\}$). Hence, instead of using analog transceiver a digital transceiver can be used for mapping the discrete time sequence, iDFT can be performed on $X[k]$. Finally using interpolation filter discrete time sequence can be converted into continuous time sequence [1]. This reduces complexity of OFDM. The function $\mathrm{sinc}(x) = \sin(\pi x)/(\pi x)$ is used as interpolation function for strictly band-limiting interpolation. Using sampling theorem,

$$x(t) = \sum_{n=0}^{N-1} x[n] \sin c((t - nT_s)/T_s). \tag{2.19}$$

However, a better signal that lessens excessive temporal side-lobes can be obtained using a root-raised-cosine filter g(t) having a small roll-off factor α or a low pass transmission filter is used.

$$x(t) = \sum_{n=0}^{N-1} x[n] g(t - nT_s) = \sum_{n=0}^{N-1} x[n] g(t - nT/N). \tag{2.20}$$

The signal generated here is a baseband signal, that can be converted to passband by,

$$s(t) = Re\{x(t)\} e^{j2\pi f_c t}$$

As per Euler's formula,

$$s(t) = x_i(t) \cos 2\pi f_c t - x_q(t) \cos 2\pi f_c t \tag{2.21}$$

Where, x_i is the real component , x_q is imaginary component and x(t) is quadrature component. Further, f_c is carrier frequency offset or can be seen as first frequency in the OFDM

channel. This passband signal needs to be down-converted at receiving end before passing through root-raised cosine filter. Considering the signal transmitted to be passband, the output is given as $y(t)$ and the AWGN by $\psi(t)$. The continuous signal at the output of root-raised-cosine filter g(-t) is converted to discrete samples by sampling. In addition, after match filtering for AWGN channel the relation between $y(t)$ and input symbols is,

$$y(t) = \sum_{n=0}^{N-1} x[n]q(t - nT/N) + z(t) \tag{2.22}$$

here $q(t) = g(t) * g(-t)$ and $z(t) = \psi(t) * g(-t)$. Addressing equation 2.20, the above equation can be expressed as $y(t) = x(t) + z(t)$. Discrete sample values $y[n]$ can be used to retrieve the data $X[k]$ by DFT.

$$y[n] = x[n] + z[n] \tag{2.23}$$

Cyclic Prefix (CP) are used in OFDM to avoid Inter Symbol Interference (ISI) . In this method a small end portion of OFDM symbol is placed identically at the starting of the signal. This creates a guarded interval before the original signal starts [19], which differentiates original signal from any part of previous signal that is received along with the needed signal. This is pictorially shown in Figure 2.7. Further, it decreases the rate of transmission depending on the length of CP. However, in general case, the length of CP (M) is less then N. In such scenario, transmission rate is negligibly affected. [1].

After addition of CP the the output samples in time domain are given by,

$$y = Hx + \psi \tag{2.24}$$

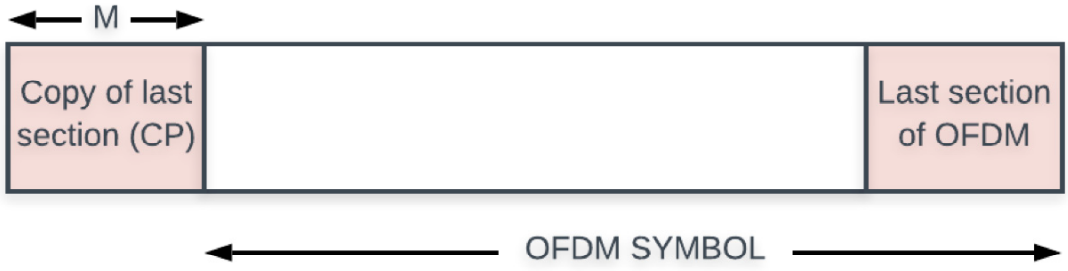

Figure 2.7: Cyclic Prefix in OFDM

where, H is a circulant matrix of dimension NXN given as,

$$H = \begin{bmatrix} f_1 & & & & f_L & \dots & f_2 \\ \vdots & f_1 & & & & \ddots & \vdots \\ \vdots & \vdots & \ddots & & & & f_L \\ f_L & \vdots & \ddots & f_1 & & & \\ & f_L & \ddots & \vdots & f_1 & & \\ & & \ddots & \vdots & \vdots & \ddots & \\ & & & f_L & f_{L-1} & \dots & f_1 \end{bmatrix} \tag{2.25}$$

In frequency domain the equation can be expressed as,

$$Y = F^H y = F^H F(y + \psi) = H^{(f)} + \psi \tag{2.26}$$

Here, the $H^{(f)}$ is a diagonal frequency gain matrix [1]

$$H^{(f)} = F^H H F = \begin{bmatrix} H[0] & & \\ & \ddots & \\ & & H[N-1] \end{bmatrix} \tag{2.27}$$

For $y = [y[0]...y[N-1]]^T$,

$$y[n] = \frac{1}{\sqrt{N}} \sum_{k=0}^{N-1} H[k]X[k]e^{j2\pi kn/N} + \psi[n] \tag{2.28}$$

These discrete samples are demodulated by taking DFT,

$$Y[k] = \frac{1}{\sqrt{N}} \sum_{k=0}^{N-1} y[n]e^{j2\pi kn/N} + \psi[n] = H[k]X[k] + \psi[k] \tag{2.29}$$

Furthermore, utilizing a filter with a frequency response inverse to that of a channel's frequency response (i.e $H_f(e^{j\omega}) = 1/H_f(e^{j\omega})$) compensation for channel distortion is done and $X[k]$ is recovered. Moreover, the underwater sound communication channels are rapidly time varying channels that implies the taps of the equivalent discrete-time channel model (Refer Figure2.6) cannot be considered to be constant for complete OFDM [1]. To account for this time variability the matrix in 2.25 is given as shown in equation 2.30.

$$H = \begin{bmatrix} f_1[0] & & & & f_L[0] & \cdots & f_2[0] \\ \vdots & f_1[1] & & & & \ddots & \vdots \\ \vdots & \vdots & \ddots & & & & f_L[n-1] \\ f_L[n] & \vdots & \ddots & f_1[n] & & & \\ & f_L[n+1] & \ddots & \vdots & f_1[n+1] & & \\ & & \ddots & \vdots & \vdots & \ddots & \\ & & & \ddots & f_L[N-1] & f_{L-1}[N-1]\cdots & f_1[N-1] \end{bmatrix} \tag{2.30}$$

2.8 Underwater Transmission System Utilizing Spreading and Interleaving over Acoustic OFDM

The transmitter system implemented in this project is combination of error control encoder, modulator and a module that converts frequency domain data into time domain (iFFT-module). The pilot sequence is similar to the preamble with period length of N_p sequence which is superimposed on the data signal with a random power value. This superposition with pilots helps to start iterative decoder and estimator process. In the experiments the data is uncoded, but it can be coded using error correction encoder. Moreover, spreading and interleaving over OFDM makes the system more sophisticated in comparison to OFDM as it can combat frequency selectivity and time selectivity.

Figure 2.8 shows transmitter system where error control encoder encodes the data which is modulated in next step, converted into time domain signal and lastly superimposed by a pilot sequence after adding a cyclic-prefix to the time domain data signal.The decoder system used in this project is an iterative decoder and, according to [20] the best results for an iterative decoder can be obtained by using one of the two error control codes, namely, LDPC codes or low rate repetition codes. However, LDPC codes are more sensitive to the power fluctuations which are more dominant in underwater acoustics communication due to the fading behaviour of the channel. Where as, in systems having repetition coding at encoder observe no such effects [1]. Although repetition coding being robust to power fluctuations has a disadvantage of less transmission rate. For the encoder used in this thesis the repetition is four times and hence have a rate $R = 1/4$. As illustrated in the figure 2.8 output of encoder is interleaved over the complete bit-frame of 2N size which is later modulated and mapped over a frame of QPSK symbols with size N.

Figure 2.9 shows the block diagram for decoupling and demodulation using iterative cancellation process. The received signal is firstly converted into frequency domain and complete decoding process takes place in Frequency domain. This received and converted

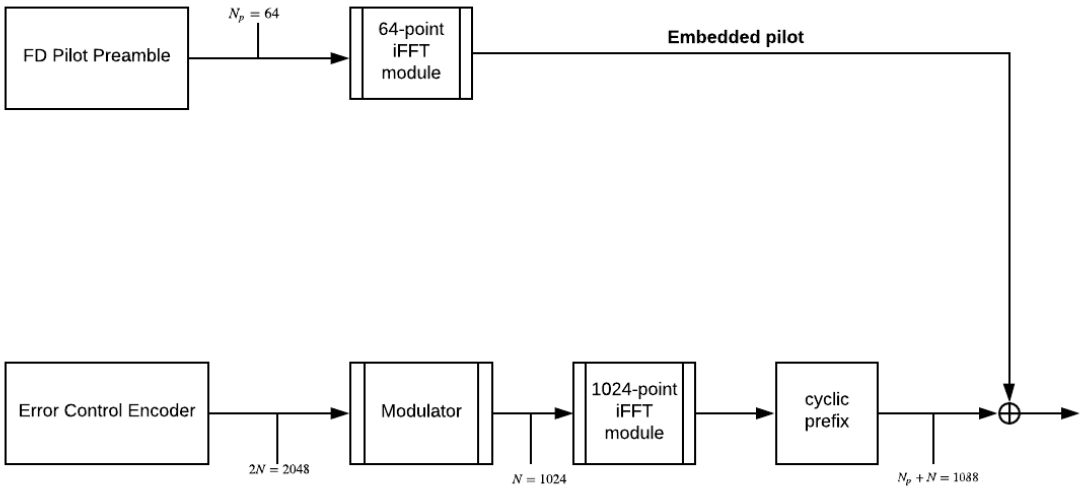

Figure 2.8: Transmitter System Block Diagram

signal is repeatedly decoded with soft-output decoder that provides LLR (Log-Likelyhood Ratios). The self-interference of non-ideal channel created by the off-diagonal elements are subtracted by using soft-bits that are mapped into real numbers ranging from -1 to 1, after encoding and modulation. Ideally, this process removes all the off-diagonal elements and produce fully diagonalized channel model after ideal number of iterations. For the experiments carried out in chapter 5, number of iterations are set to 100. This decoder is explained in detail in [21], [20], [22] and operational examples are given in [23].

The reason behind employing this type of decoder is, the channel capacity for a channel having random interference can be attained by the given setup with possible application of spatial coupling [22]. Moreover, for a performance of high capacity, high rate repetition coding or low rate LDPC codes are required according to [20]. However, fading within OFDM frames might cause failure of signal at receiving end in LDPC codes. Hence, repetition coding is preferred in this project.

Considering Y to be the output signal from the channel that can be given as,

$$Y = HX + n \tag{2.31}$$

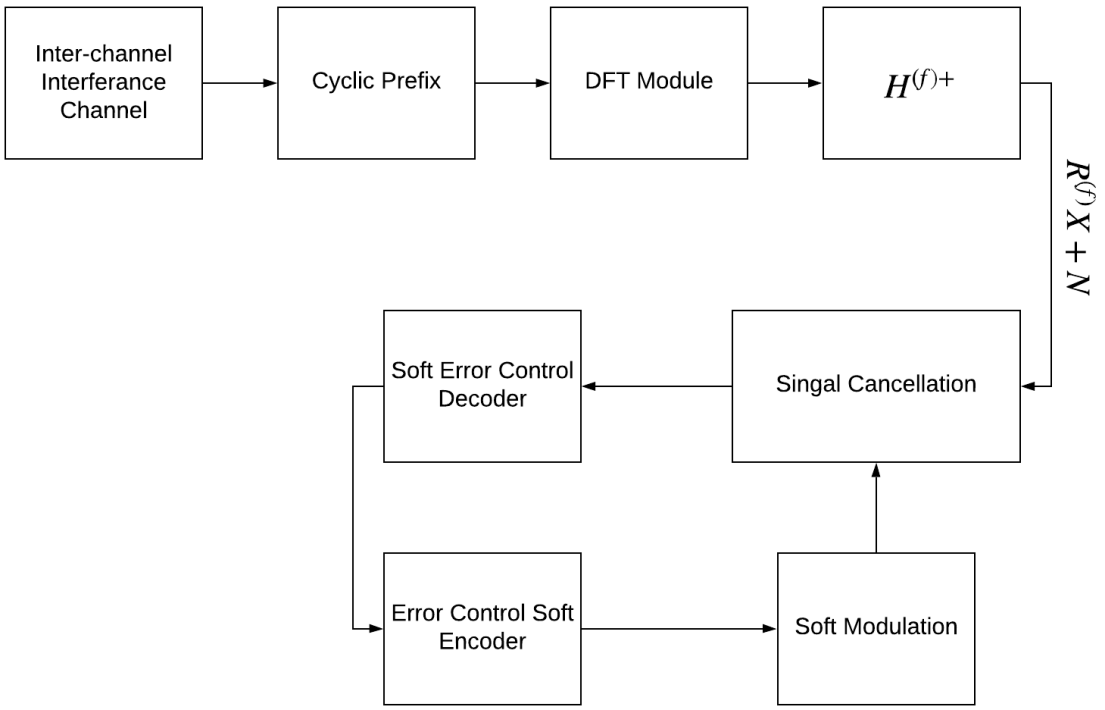

Figure 2.9: Iterative Decoder block Diagram

where, H is the channel matrix in frequency domain which is known to the user, n is the noise and X is the data which needs to be determined. The receiver system can be mathematically explained as below.

Initially the received signal is multiplied by Hermitian matrix $(\bar{H}^*)$ for the purpose of match filtering,

$$\bar{H}^* Y = \bar{H}^* (HX + n) \tag{2.32}$$

$$\bar{H}^* Y = \bar{H}^* H\ X + \bar{H}^*\ n \tag{2.33}$$

$$Y_F = RX + n' \tag{2.34}$$

this can be expanded as,

$$Y_F = R_{\text{diag}} X + R_{\text{off}-\text{diag}} X + n' \tag{2.35}$$

Here, $R_{\text{diag}}X$ is the required signal, $R_{\text{off}-\text{diag}}X$ is the data with high interference that needs to be removed and n' is the noise after filtering.

Further, the output bit LLRs obtained from soft-decoder are converted into soft bits that are later modulated into soft symbols which are denoted as $\widetilde{X}$. Now, utilizing the repeated cancellation process the iterative receiver provides an iterative estimated sequence. This can be symbolized as $Y^{(i)}$ and is given as,

$$Y^{(i)} = Y_F - R_{\text{off}-\text{diag}}\widetilde{X}^{(i)} \tag{2.36}$$

$$Y^{(i)} = R_{\text{diag}}X + R_{\text{off}-\text{diag}}(X - \widetilde{X}^{(i)}) + N \tag{2.37}$$

Multiple iterations (number of iteration are fixed) of 2.37 and 2.32 takes place. Higher the convergence of X towards $\widetilde{X}$ lower the interference. Moreover, if $X \rightarrow \widetilde{X}$ the off diagonal elements are completely canceled and ideal zero interference performance is achieved.

2.9 Estimator

The estimator model used for this project is Forward-Backward Kalman Filter discussed in [24] and [1]. Here, channel estimation can be conducted in two ways, first way is by estimating channel response matrix (H) in time domain, where as second way refers to obtaining frequency domain matrix after match filtering (R). The mathematical relation between this two matrices is explained in equation 2.34 and 2.33. The estimator is created by developing the optimal MMSE estimator, then time variation of channel is added with the help of AR(1) state-space equations. This AR(1) model is then used with linear observations to create a kalman filter estimator. Lastly, for a refined solution Rauch-Tung -Striebel smoother and optimal combining algorithm are used which is known as forward-backward kalman filter. The performance improvements are noted in terms of Mean Square Error

(MSE) or Residual Error (RE). It should be noted that although the frequency domain matrix R is more convenient for signaling, but the estimation process completely takes place in time domain due to the lack of frequency domain transformed statistical modeling techniques that are considered in this literature for evolution of channel impulse response with time.

Here the main aim is to estimate the time domain matrix H as illustrated in 2.25 with the help of liner observations $Y = H^{(f)}X + N$, Log likelyhood Ratios LLRs (X) and other known information of the channel. Figure 2.10 depicts the process for estimation with a simple block diagram.

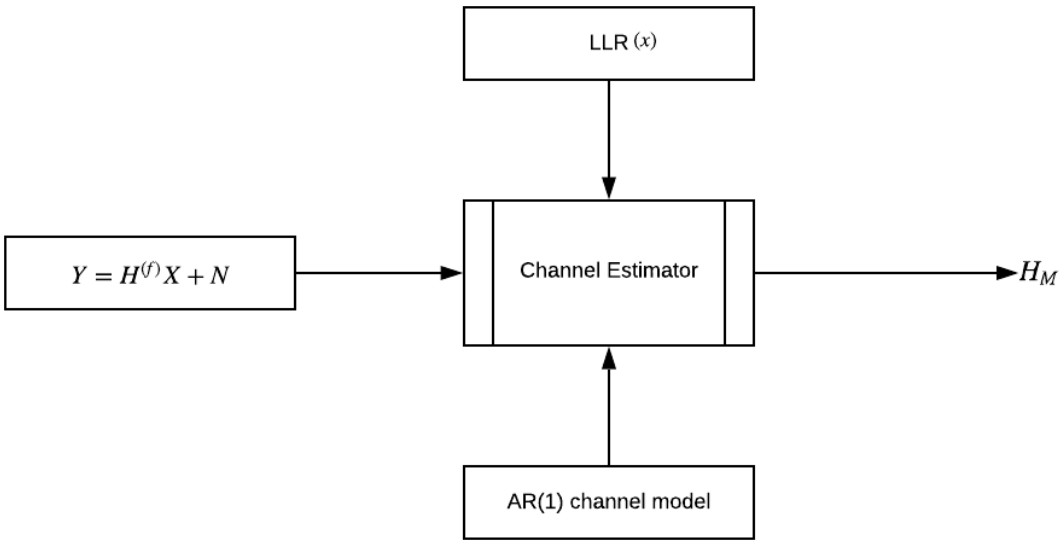

Figure 2.10: Estimation Process Block Diagram to attain estimation of channel H_M

The pilots-only MMSE channel can be portrayed as,

$$H_M = \arg\min \mathbb{E}_{\widetilde{H}} \left\{ |\widetilde{H} - H|_F^2 |y| \right\} \tag{2.38}$$

As H is nothing but matrix with impulse responses t different time interval,

$$H_M = \arg\min \underset{\widetilde{f}[i]}{\mathbb{E}} \left\{ |\widetilde{f}[i] - f[i]|^2 |y| \right\} \tag{2.39}$$

where, F is forbenius norm, and $\widetilde{H}$ and $\widetilde{f}[i]$ are optimization variables.

Solving equation 2.39 leaves us with a MMSE estimator of the form,

$$H_M = \mathbb{E}_{\mathrm{H}} \left\{ H|y \right\} \tag{2.40}$$

$$f_M = \mathbb{E}_f[i] \left\{ f[i]|y \right\} \tag{2.41}$$

Estimators in equation 2.40 and 2.41 are pilots-only estimators, which means the pilot symbols are already known at the receiver. The channel estimator in expression 2.41 needs the channel impulse responses at various time from 0 to N. Therefore, it utilizes the past observations in the interval [0 to i] and the future observations in the time interval $[\mathrm{i}+1 \text{ to } \mathrm{N}]$. There are two ways to approach this. In the first method known as two step estimation strategy, firstly channel is estimated using past observations only and then using future observations only. Further in second step this two estimates are combined. This can be expressed as,,

$$\bar{f}[i] = \mathbb{E}_{f[i]} \left\{ f[i]|f_{forward}[i], f_{backward}[i] \right\} \tag{2.42}$$

Second approach to acquire channel impulse response, is applying a smoother to calculate forward estimates. For this methodology, a state space model is developed.

State space model when used with the linear observations model a basic kalman filter can be developed. In this thesis, first order auto-regressive model is utilized. This model

can be described as,

$$\begin{bmatrix} f_1[i] \\ f_2[i] \\ \vdots \\ f_L[i] \end{bmatrix} = \begin{bmatrix} a_{AR(1)} & 0 & \cdots & 0 \\ 0 & a_{AR(1)} & \cdots & 0 \\ \vdots & \cdots & \cdots & \vdots \\ 0 & 0 & \cdots & a_{AR(1)} \end{bmatrix} \begin{bmatrix} f_1[i-1] \\ f_2[i-1] \\ \vdots \\ f_L[i-1] \end{bmatrix} + \begin{bmatrix} v_1[i] \\ v_2[i] \\ \vdots \\ v_L[i] \end{bmatrix} \tag{2.43}$$

where, $f_n[i]$ are active taps at n position of channel impulse response $f[i]$, $v_n[i]$ is Gaussian noise of AR(1) process respective to n^{th} tap. In this process we assume that taps are uncorrelated to each other. The channel taps are obtained using SOS (Sum-of-Sinusoids) model as below,

$$f_n[i] = \sqrt{\frac{P_n}{M}} \sum_{m=1}^{M} e^{j(\phi_m + 2\pi f_m i T_s)} \tag{2.44}$$

Here, P_n represents power of respective tap obtained from Power Delay Profile (PDP) of the channel. To find the $a_{AR(1)}$ parameters, auto-correlation function of the taps is fitted to the auto-correlation function of assumed AR(1) model. Suppose $Z_n(m)$ is the auto-correlation for n^{th} tap according to AR(1) model,

$$Z_n(m) = \mathbb{E}\, f_n[i] f_n^*[i+m] = Z_{n,tr}(0) a_{AR(1)}^m \tag{2.45}$$

Where as, the auto-correlation function following SOS (Sum-of-Sinusoids) for n^{th} tap,

$$Z_{n,sos}[m] = \frac{P_n}{1 + (2\pi m \alpha T_s)^2} \tag{2.46}$$

where α is the Doppler spread coefficient as described in equation 2.3 and T_s is sampling time. Therefore, $a_{AR(1)}$ can be given as,

$$a_{AR(1)} = \arg\min_{\bar{a}_{AR(1)}} \sum ||Z_n[m] - Z_{n,sos}[m]||^2 \tag{2.47}$$

In the experiments pilots-only estimation is utilized which supposes that the signal bares no data. Channel evolution can be observed with the help of linear observation model given by expression 2.48 and state-space model represented in 2.49.

$$y[i] = f[i]x + n[i] \tag{2.48}$$

$$f[i+1] = A^{(1)} f[i] + v[i] \tag{2.49}$$

Structure of forward-backward Kalman filter for AR(1) can be explained with the set of Kalman filter equations:

$$\sigma_e^2[i] = \sigma_n^2 + x * \mathrm{M}_f[i|i-1]x \tag{2.50}$$

$$K_f[i] = \frac{\mathrm{M}_f[i|i-1]x}{\sigma_e[i]^2} \tag{2.51}$$

$$e[i] = y[i] - \mathbf{f}_f[i|i-1]x \tag{2.52}$$

$$\mathbf{f}_f[i|i] = \mathbf{f}_f[i|i-1] + K_f[i]e[i] \tag{2.53}$$

$$\mathbf{f}_f[i|i+1] = \mathrm{A}^{(1)}\mathbf{f}_f[i|i] \tag{2.54}$$

$$\mathrm{M}_f[i|i] = \frac{\mathrm{M}_f[i|i-1]xx * \mathrm{M}_f[i|i-1]}{\sigma_e[i]^2} \tag{2.55}$$

$$\mathrm{M}_f[i+1|i] = \mathrm{A}^{(1)H}\mathrm{M}_f[i|i]\mathrm{A}^{(1)} + \mathrm{Q}^1 \tag{2.56}$$

Here, f as a subscript stands for forward estimates and $\mathrm{M}_f[i]$ is its accuracy of estimation. Such similar set of equations is used for backward estimates with a subscript of b. The forward Kalman filter runs for the time $i = 0$ to N whereas, the backward filter runs from $i =$ N to 0.

$$\mathrm{M}_f[i+1|i] = \mathrm{M}_f[i|i] \tag{2.57}$$

The above equation (2.57) is satisfied at steady state condition. This implies that the Kalman filter has reached to a position where no further improvement in the estimate can be obtained. At this stage the equation 2.56 can be depicted as,

$$\mathrm{M}_f = \mathrm{A}^H \mathrm{M}_f \mathrm{A} + \mathrm{Q} \tag{2.58}$$

which is a discrete time Lypnov equation with solution,

$$\mathrm{M_f} = \sum_{k=1}^{\infty} (\mathrm{A}^H)^k \mathrm{Q} \mathrm{A}^k \tag{2.59}$$

After deriving forward and backward estimates we still do not have all the available observations for channel estimation. This can be solved in two ways, firstly by using a Raunch-Tung Sriebel Smoother which is applied on backward pass while having forward Kalman filter. In order to produce new estimates, the kalman smoother considers the model matrices, and it is the global minimum to the following error function [25].

$$J_k(f_i) = ||\tilde{f}_f[i+1|N] - A^{(1)} f_f[i|N]||^2_{Q-1} + ||f_i - \tilde{f}_f[i|i]||^2_{M_f[i|i]} \tag{2.60}$$

The smoothed estimate of the channel at time i for all N observations is

$$f^s[i|N] = \arg\min_{f_i} J_k(f_i) \tag{2.61}$$

The solution to equation 2.61 is the Rauch-Tung-Striebel smoother, given as,

$$f^s[i|N] = \tilde{f}[i|i] + C[i](f^s[i+1|N] - \tilde{f}[i+1|i]) \tag{2.62}$$

$$\mathrm{M}^s[i|N] = \mathrm{M}_f[i|i] + \mathrm{C}[i](\mathrm{M}^s[i+1|N] - \mathrm{M}_f[i+1|N] - \mathrm{M}_f[i+1|i])\mathrm{C}^T[i] \tag{2.63}$$

$$\mathrm{C[i]} = \mathrm{M_f[i|i]A^{(1)T}M_f[i+1|i]^{-1}} \tag{2.64}$$

Here, $f^s[i+1|N] - \tilde{f}[i+1|i]$ is innovation noise and $\mathrm{C}[i]$ is certainty matrix. In other approach, we use two Kalman filters one runs forward and second runs backward. Both forward and backward filters have the same steady state estimation errors and the corresponding optimal combiner mean square error is then

$$\mathrm{M} = \frac{1}{2}\sum_{k=1}^{\infty}(\mathrm{A}^H)^k \mathrm{Q}\mathrm{A}^k \tag{2.65}$$

$$\mathrm{MSE} = \mathrm{Trace}(\mathrm{M}) \tag{2.66}$$

Chapter 3

Theory Behind Wide-Band SOS model

As discussed in chapter 2 both the models , that is, the narrow-band model and the wide-band mode revolve around the theory of sum-of-sinusoids (SOS) [26] and are SIMO (Single Input Multiple Output) models. However, wide-band model being frequency dependent it has same calculations for different set of frequencies and are collaborated at then end to get a result. This is discussed in detail further. Spatial correlation of channel impulse response is required to monitor and understand a MIMO (Multiple Input Multiple Output) system. This channel correlation affects capacity of resulting and MIMO communication algorithms like beamforming [27] and equalization [9]. The primary aim of this channel model is the analysis and simulation of the designed system to understand the possible resistances cased due to various underwater factors with better accuracy and sensitivity with reference to changing frequency of Bandwidth and not retrieving the exact signal. Also, this model provides closer results to the real life channel due to consideration of path specific Doppler shifts.

The complete modeling and estimation system is combination of three steps. First, power-delay profile is generated using Bellhop specific to input parameters of the system under test. Second step involves generation of channel matrix which is then used in third step to transmit a signal with Orthogonal Frequency Division Multiplexing (OFDM) modulation technique finally providing MSE (Mean Square Error) or Residual Error (RE) and BER (Bit Error Rate) of the channel using estimated channels which is discussed in upcoming chapter. Thus, this section provides theory of wide-band model and mathematical modeling that is used in chapter 4 for implementation.

3.1 Concept of Frequency Dependent/ Wide-Band Model

Referring to Figure 2.4, Delay power profile input block will have the same working as narrow-band model. However, Doppler spread profile for different frequencies of bandwidth will be variable as the higher frequencies have higher Doppler spread than lower ones. To consider this frequency dependent behaviour of Doppler spread, this project divides the actual bandwidth of the system in small k number of sub-band addressed as packets here. Though, ideally the splitting should generate one channel for each frequency, this being very complex and impractical approach, the splitting here is done in such a way that each packet will contain frequency values that are near by and which will not bring a significant change in Doppler spectrum of Doppler frequencies. Finally, Doppler spread frequencies will be derived for each packet separately, taking into consideration only the effect of carrier frequency of that particular sub-band. This will create necessary spreading of Doppler spectrum for different range of frequencies, giving more accurate results. This concept can be better understood with the Figure 3.1

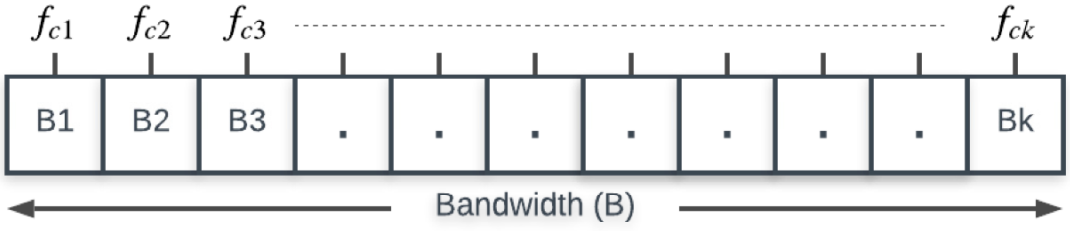

Figure 3.1: Band division model

In the above figure, B1, B2 ..... Bk are k sub-bands (packets) of the original bandwidth B. k is an input parameter that can be given by the user depending on the bandwidth of the system and accuracy expected by the user. More the number of band closer the results to the real life channel. However, increasing number of bands increases the complexity of the model. Therefore, it is a trade between complexity and accuracy that should be

wisely decided by the user. Further, $f_{c1}, f_{c2}, ...f_{ck}$ are the carrier frequencies of each band separately calculated.

3.2 Mathematical Computations for Wide-Band Model

Considering Figure 2.4 for the case of dependent model instead of $x_i(t)$, $x(t)$ are considered complex transit samples, as shown in figure 3.2 which are divided into k sub-samples, where k is number of packets (sub-bands). As discussed above the packets are made form dividing frequency band into smaller sub-bands which in-turn makes it necessary to divide the sending data into similar packets respective to each band for further transmission over the channel. Here, the samples corresponding to each band will be $x_1(t), x_2(t), ..., x_k(t)$. The filter model can be diagrammatically represented as in figure. The $x(t)$ samples can be expressed as,

$$x(t) = \sum_{i=1}^{k} x_i(t) \tag{3.1}$$

These samples enter the fading channel in Figure 3.2. The output $Z(t)$ is obtained after processing through transmitter pulse shaping filter with g(t) as its impulse response, further passing through channel, adding white noise and finally summing together the outputs from each receive filter. The system formed here is discrete linear time-varying filter, that is

$$f_i(t;\tau) = h_{p,i}(t;\tau) * g(\tau) * g(-\tau) \tag{3.2}$$

Where, $i = 1, ..k$, that means there will be total k number of equations using equation 3.2 that will be finally summed up for the output. Also, $h_{p,i}(t;\tau)$ for frequency dependent channel using equation 2.7 can be given as,

$$h_{p,i}(t;\tau) = \sum_{P=1}^{P} c_{p,i}(t)\delta(\tau - T_p) \tag{3.3}$$

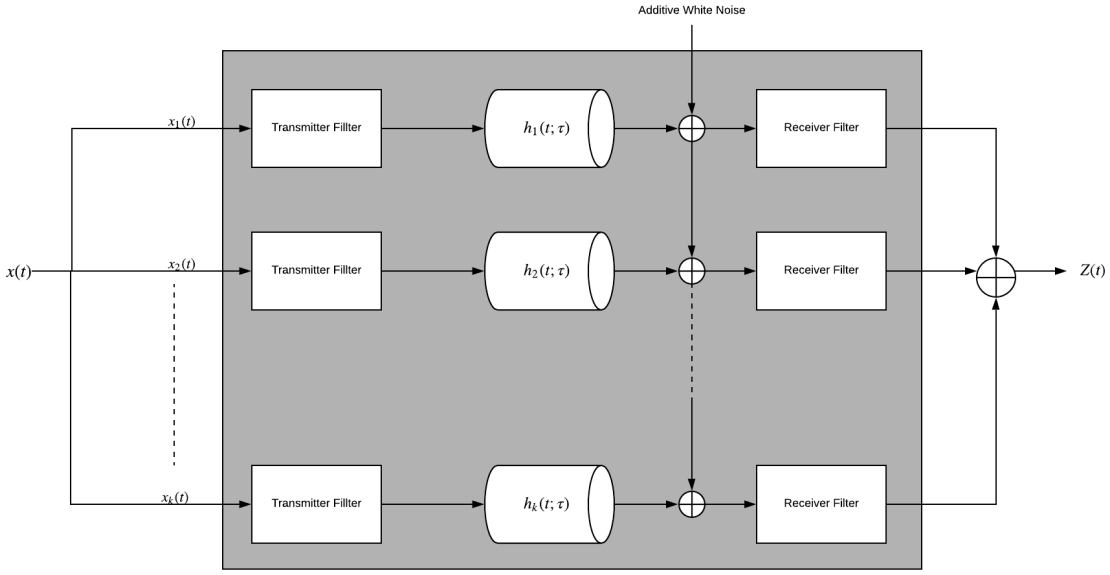

Figure 3.2: Filter model for wide-band channel model

This equation will be used k number of times to get the value of $h_{p,i}(t;\tau)$ for all the packets.From the equation 2.6

$$h[i]_{i\text{Rayleigh}} = \frac{1}{\sqrt{M}} \sum_{m=1}^{M} e^{j(\phi_m + 2\pi f_{m,i} T_s)} \tag{3.4}$$

Here, T_s is sampling time and as it can be seen in the above equation Doppler frequencies are different for each packet. They can be mathematically understood as,

$$f_{m,i} = f_m.a_i \tag{3.5}$$

Here, a_i is a scaling coefficient that can be given as the ratio of the carrier frequency of the respective packet in operation to the carrier frequency of complete bandwidth.

$$a_i = \frac{f_i}{f_c}, \tag{3.6}$$

where, $f_i = f_{c1}, ..., f_{ck}$. This will also generate $'i'$ number of $h[i]_{i\text{Rayleigh}}$ that is, one for

each packet.

Now, Considering the time varying taps case. Using the same tapped delay line model in Figure 2.6 $f_l[K]_{\text{Rayleigh}}$ will be generated k times making equation 2.11 frequency dependent, which can be given by using equation 3.3 and 3.4 as follows:

$$f_l[k]_{\text{Rayleigh}} = \frac{1}{\sqrt{M}} \sum_{m=1}^{M} e^{j(\phi_m + 2\pi f_{m,i}(kT_s - \tau_m))} * g_{\text{total}}(lT_s - \tau) \tag{3.7}$$

The output $Z(t)$ can be expressed as,

$$Z(t) = \sum_{i=1}^{k} Z_i(t) + n(t) \tag{3.8}$$

$Z_i(t)$ is output per packet that is summed over $'i'$ where $i = 1...k$ and can be mathematically expressed as,

$$Z_i(t) = f_i(t;\tau) * x_i(t) \tag{3.9}$$

Hence, the output for time varying taps can be written using equation 3.9 and 2.10 by,

$$Z_k = \sum_{i=1}^{K_s} \sum_{l=1}^{L} x_{k-l,i} f_{l,i}(KT_s) + n_k \tag{3.10}$$

3.2.1 Computation of Phase shifts

In the narrow-band model (Frequency independent model) the phase selection which is frequency dependent is constant as there exists singular carrier frequency. However, as discussed in Figure 3.1 to make this model wide-band each packet has its own carrier frequency. Phases here are the combination of initial phase and the shifts due to delays that can be represented as follows [1]:

$$Phases = \rho_{in} + 2\pi f_c T_s \tag{3.11}$$

For k frequency bands Considering 'k' number of packets, the phases for each packet can be found using following general formula, for $i = 1, 2, ..k$

$$Phase_i = \rho_{in} + 2\pi f_i a_i \delta T_s, \tag{3.12}$$

Here, 'a' can be given as the ratio of the carrier frequency of the packet in operation to the carrier frequency of complete bandwidth.

$$a_i = \frac{f_i}{f_c}, \qquad f_i = f_{c1}, ..., f_{ck} \tag{3.13}$$

where, f_c is the carrier frequency of complete bandwidth, as mentioned in equation 3.6.

In order to describe an example for expansion of the above equation, phases for first two packets are derived below,

$$Phase_1 = \rho_{in} + 2\pi f_{c1} a_1 \delta T_s, \tag{3.14}$$

where $a_1 = f_{c1}/f_c$.

$$Phase_2 = \rho_{in} + 2\pi f_{c2} a_2 \delta T_s, \tag{3.15}$$

where $a_2 = f_{c2}/f_c$.

3.3 OFDM over Wide-band Channel Model

Here we derive a mathematical representation of OFDM transmission over wide-band channel model. Since different sub-carriers belong to different sub-bands addressed in the model we derive a representation analogous to Section 2.7 but for each sub-band.

Considering that the frequency band is divided into 'k' packets, the output for each packet can be written as $Y_1 ... Y_k$ where every output will have its own matrix with 'n/k' number of frequencies if the frequencies range from $f_1 .... f_k$. Hence, the total output of the

channel denoted by Y can be given as,

$$Y = (Y_1 + Y_2 + ...Y_k) + N \tag{3.16}$$

Each output is generated by multiplying the H matrix formed for every sub-band (This matrix is described in equation 3.21) with the respective data packet X_i and a Fourier transform matrix F. This can be noted as,

$$Y_i = F^H H_i F \cdot X_i, \qquad i = 1, 2.., k \tag{3.17}$$

The data matrix X_i can be procured by splitting the complete data matrix into k data packets with each packet having n/k number of values. Considering an example for first data packet X_1 can be written as,

$$X_1 = \begin{pmatrix} x_1 \\ . \\ . \\ . \\ x_{n/k} \\ 0 \\ 0 \\ 0 \end{pmatrix}$$

Note that rest of the values in the matrix are set to zero. Generalized form of the above

matrix, without zeros can be given by,

$$X_{l_{sub}} = \begin{pmatrix} V_s \\ \vdots \\ V_e \end{pmatrix}$$

Where, $l = 1, .., k$;

The above matrix is a sub-matrix that contains the elements with values in it, that is, it does not have zero elements as this matrix represents a generalized form of a sub matrix that corresponds to the data for current frequency band. V_s is the value of data at position $Start_P$ as given in expression 3.18 and V_e is the value of data at position End_P as represented in equation 3.19. These values will be positioned between $Start_P$ and End_p and rest all the positions will hold zero as its value. The positions for each packet are determined by,

$$Start_P = [(l-1) \times \frac{n}{k}] + 1, \tag{3.18}$$

$$End_P = Start_P + \frac{n}{k} \tag{3.19}$$

The complete matrix will comprise this sub matrix from position $Start_P \; to \; End_P$

$$X_l = \begin{pmatrix} 0 \\ 0 \\ 0 \\ \vdots \\ X_{lsub} \\ 0 \\ \vdots \\ 0 \end{pmatrix} \tag{3.20}$$

The cyclic matrix for each packet needs to be calculated to get the output Y as outlined in expression 3.17. Moreover, the circulant matrix from equation 2.30 has been presented in generalized form for wide-band model (in equation 3.21) in such a way that is is dependent on sub-bands. That directs towards an independent circulant matrix for each sub-band which will lastly be added to give a final matrix as expressed in equation 3.23.

$$H_i = \begin{bmatrix} f_{1i}[0] & & & & f_{Li}[0] & \cdots & f_{2i}[0] \\ \vdots & f_{1i}[1] & & & & \ddots & \vdots \\ \vdots & \vdots & \ddots & & & & f_{Li}[n-1] \\ f_{Li}[n] & \vdots & \ddots & f_{1i}[n] & & & \\ & f_{Li}[n+1] & \ddots & \vdots & f_{1i}[n+1] & & \\ & & \ddots & \vdots & \vdots & \ddots & \\ & & & \ddots & f_{Li}[N-1] & f_{L-1i}[N-1]\cdots & f_{1i}[N-1] \end{bmatrix} \tag{3.21}$$

Where, i= 1,...,k The output is,

$$Y = Y_1 + Y_2 + ... + Y_k + N \tag{3.22}$$

This can be further expanded as,

$$Y = F^H[H_1FX_1 + H_2FX_2 + ... + H_kFX_k] + N \tag{3.23}$$

An example of one such circulant matrix is shown in Figure 3.3. The diagram depicts the mesh plot of 'H' matrix in time domain for a underwater system with bandwidth of 320 Hz and 1024 as its carrier frequency. The matrix presented in the figure is obtained from narrow-band model. Where as, the wide-band model generates 'k' such channel matrices as each sub-band has its own channel which are finally summed to get the final channel. This summation takes place in frequency domain as represent in equation 3.23.

Moreover, figure 3.4 portrays how the SOS samples obtained from equation 3.4 vary in

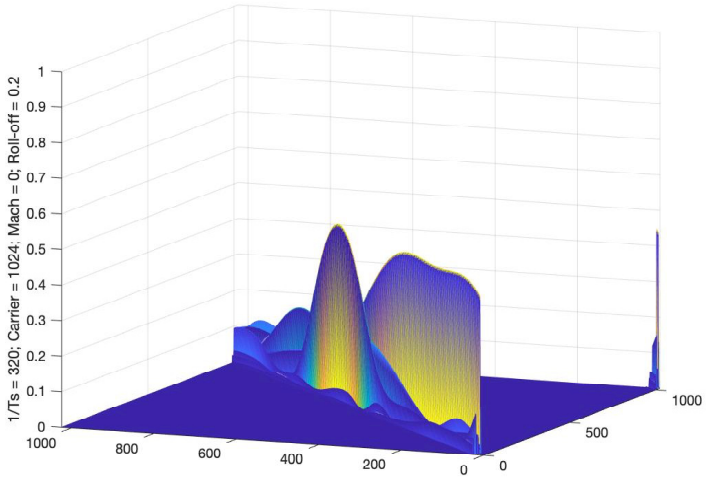

Figure 3.3: Mesh Plot of Circulant matrix $\|H\|$ in time domain

time for different packets. It is evident from this figure that the SOS samples of packet3 changes faster than samples in packet2 and packet1. This implies it has greater spread than other channels in frequency domain. In other words, spread of channel for packet3 $>$ the spread of channel for packet2$>$ The spread of channel for packet1.

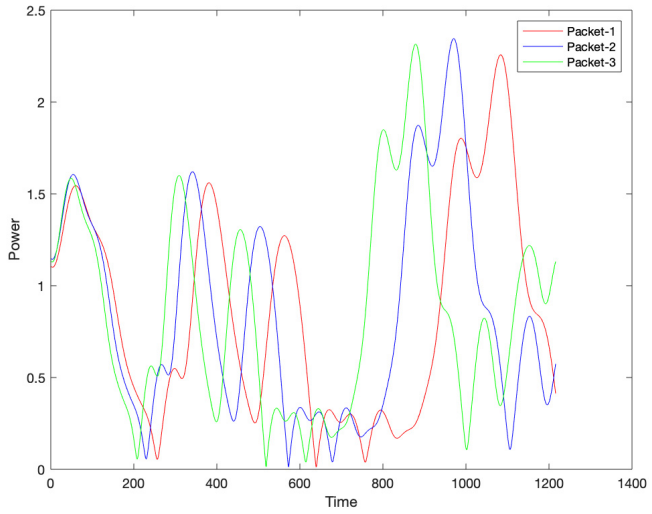

Figure 3.4: Sum-of -Sinusoid samples in Time domain

Chapter 4

Algorithmic and Software Implementation of the Channel Model

Implementation of SOS wide-band channel with OFDM signaling is demonstrated in this section. For a complete transmission process of a signal using the concepts reviewed in chapter 3 there exists three sections of Programming. This complete flow is shown in the Figure 4.1. As depicted in the figure, first section acts on collecting the system parameters required to generate channel. This step is processed using Bellhop. Input to Bellhop is user give as it includes SSP (Sound Speed Profile) that is measured during experiments in same ocean environment, depth of receiver, transmitter receiver distance and other parameters of the system designed available to user. Further, the data generated in Bellhop is fed in MATLAB where the channel matrix H is generated. In the case of wide-band model multiple channel matrices $H_1, H_2, ...H_k$ are generated corresponding to k sub-bands. Lastly, these channels are used to transmit respective data packet as represented in equation 3.23. This last process takes place in the Simulink model. Moreover, simulink model also performs iterative channel estimation as reviewed in literature [24]. Finally computing Mean Square Error (MSE), Residual Error (RE) and Bit Error Rate (BER) to test the quality of channel.

4.1 Flow Diagram for MATLAB Program

MATLAB program generating the channel is constructed as shown in the block diagrams of this section. This program holds one main file and rest are the function files. The Block diagram of main file is represented in white and rest of the function files are represented by particular colour for simplicity of understanding.

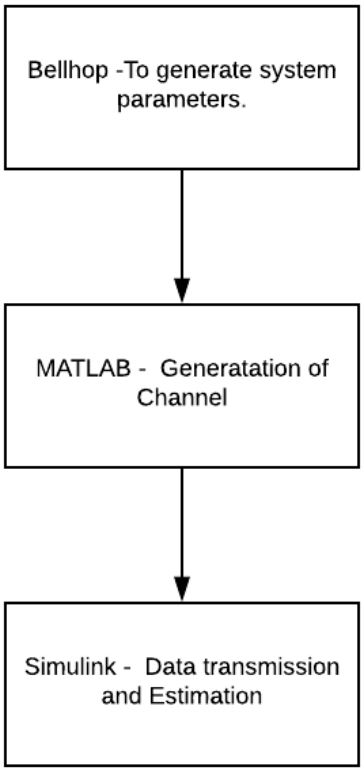

Figure 4.1: Implementation Block Diagram

Figure 4.2 and 4.3 represent the flow of main program. Thus, as shown in first block bellhop file is loaded. Further, few more system parameters like carrier frequency, bandwidth are to be set and some of them are to be calculated from the data in bellhop file in desired form. For example, angle of arrivals in radian, path power in sequence where the path with least delay is stored first. Furthermore, as mentioned earlier the number of packets, i.e, how many sub-bands to be created of the complete bandwidth is to be decided by the user by making a trade between complexity and accuracy. However, for a bandwidth as narrow as 320 Hz when tested by dividing the bandwidth into 3 sub-bands, generates improved and more realistic results with less complicated and practical way. After deciding the number of sub-bands, all the frequencies are distributed per packet and then carrier

frequency per packet is calculated. Along with carrier frequencies, path delays, Doppler spread parameter α is evaluated using number of top bounces from loaded Bellhop file. Further, frequency dependent Doppler spread factor that is represented by 'a' in equation 3.13 is calculated for every packet. A function file for calculation of Delays and phase shifts is called in the main program (This file is represented by green blocks in block diagram). Once the function file is done computing, the main program takes SOS and OFDM parameters into consideration like number of sinusoids used to construct the impulse response, number of samples utilized in OFDM, length of cyclic prefix and so on. Initial states to compute SOS samples is set in the function file discussed in block diagram with yellow blocks. The last function file (represented by blue blocks) generates SOS samples which are ultimately used to generate channel matrices in the main program.

Figures 4.4, 4.5 and 4.6 represents an algorithm for working of function files generating delays and phases, setting initial state and computing SOS samples respectively. Firstly, referring Figure 4.2, to calculate delays and phases, it is checked if any values are stored previously under same variable names. If so the variables are emptied and the path is set to 1. Now, for all the paths, delays are calculated using a for loop and after each loop calculated delays are stored in the emptied variable. Further, Phases are calculated as summation of initial phases and phase shifts due to delays. As, mentioned in equation 3.12 they are a function of carrier frequency which is different for each band in the case of wide-band model. Hence, phases are calculated for all the packets and are finally stored before returning to the main program.

Discussing about the next function file that sets the initial state for calculation of SOS samples in next function file and is represented in Figure 4.3, it can be observed that a pulse shaping grid is setup in first block. The pulse shaping filter used in this model is RC type filer. Hence, in next block RC pulse is generated separately for zeros and non-zeros. Further, random Doppler frequencies and phases are generated for every path. Here,

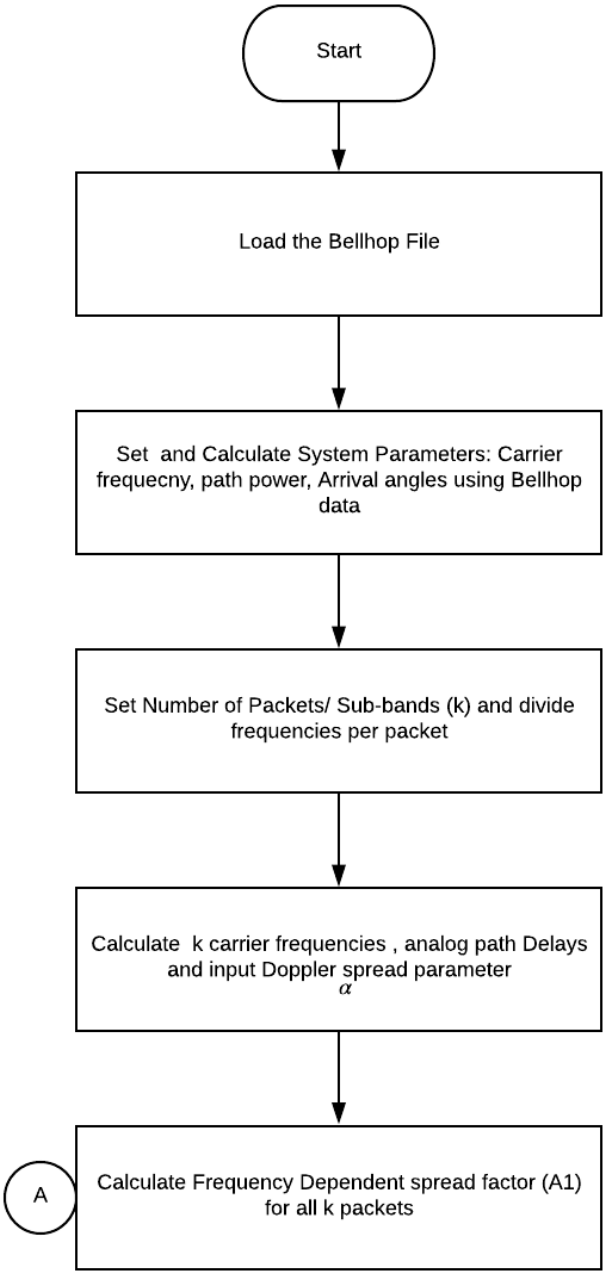

Figure 4.2: Block diagram of Main Program-1

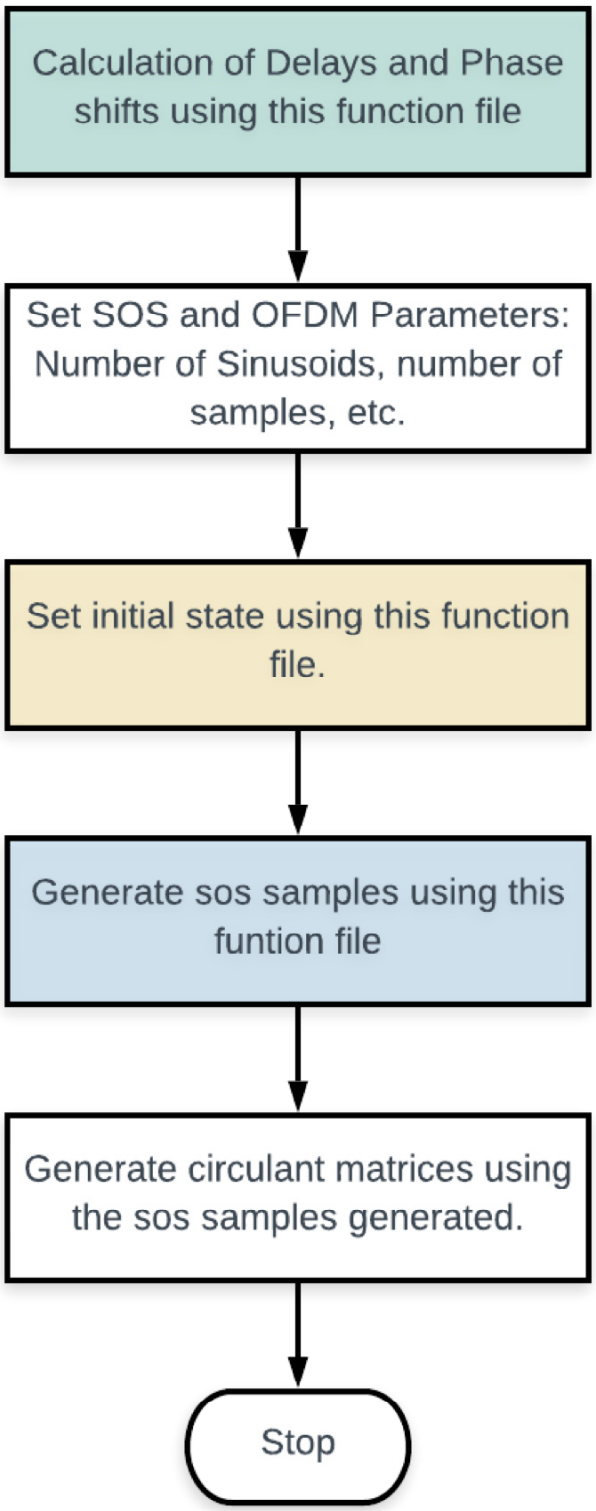

Figure 4.3: Block diagram of Main Program-2

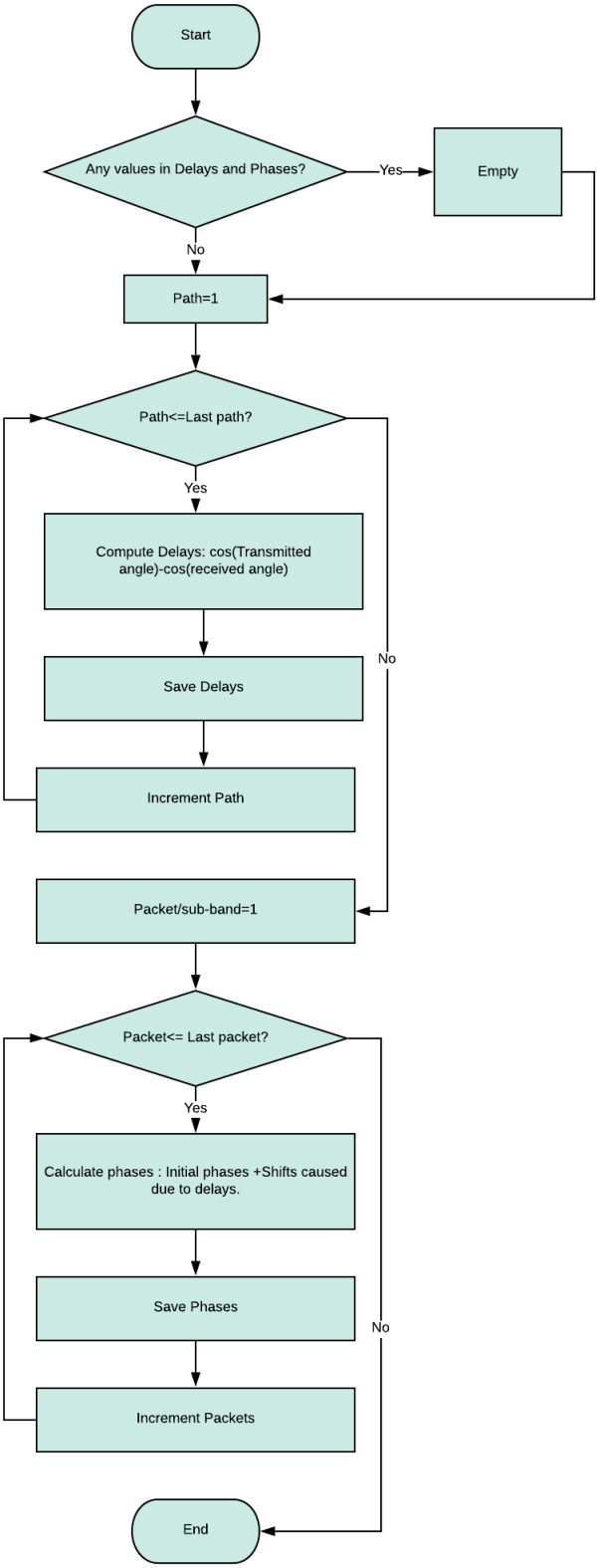

Figure 4.4: Function file for Delays and Phases

Doppler frequencies are generated using equation 2.5. In next step Doppler spread and Doppler shifts are added for every packet. Also, calculation for 'Delta t'- a shift increment factor for each sample of each path is performed. Now, for every packet final phases are generated and saved by addition of random phases and phases generated in function file illustrated in 4.4. Next, computation scaling coefficient for SOS samples that constitutes of SOS scaling parameter $1/\sqrt{M}$ and amplitude of the paths occurs. Lastly, create empty arrays to store fading and SOS samples.

In the final function block, fading power per path is calculated. Now, utilizing this data and presets from previous function file SOS samples are generated. These samples are further used to generate channel matrices in main program. SOS samples here are determined using Equation in 3.4. Lastly, after returning to the main program empty array for circulant matrix H is created and is further filled by generating H matrices for each packet with the help of SOS samples, Nyquist samples and path amplitudes. This H matrix is referred as channel matrix.

4.2 Brief on Simulink Program

In order to test the channel generated, the channel matrices H are combined with data to generate output as shown in expression 3.23. For this process to take place a simulink model discussed in [1] is utilized, which is represented by block 3 in Figure 4.1. Moreover, this simulink not only preforms the above mentioned task but also computes MSE, RE and BER of the given system.

4.3 Simulink Estimation model

Figure 4.7 shows the block diagram explaining the basic working of this model.

Function of each block is discussed as follows,

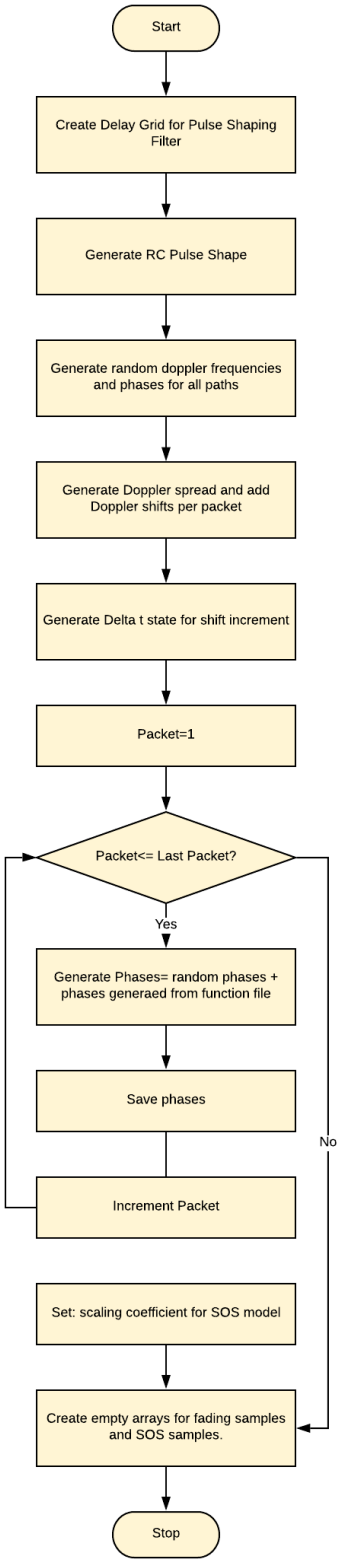

Figure 4.5: Set Initial State Function File

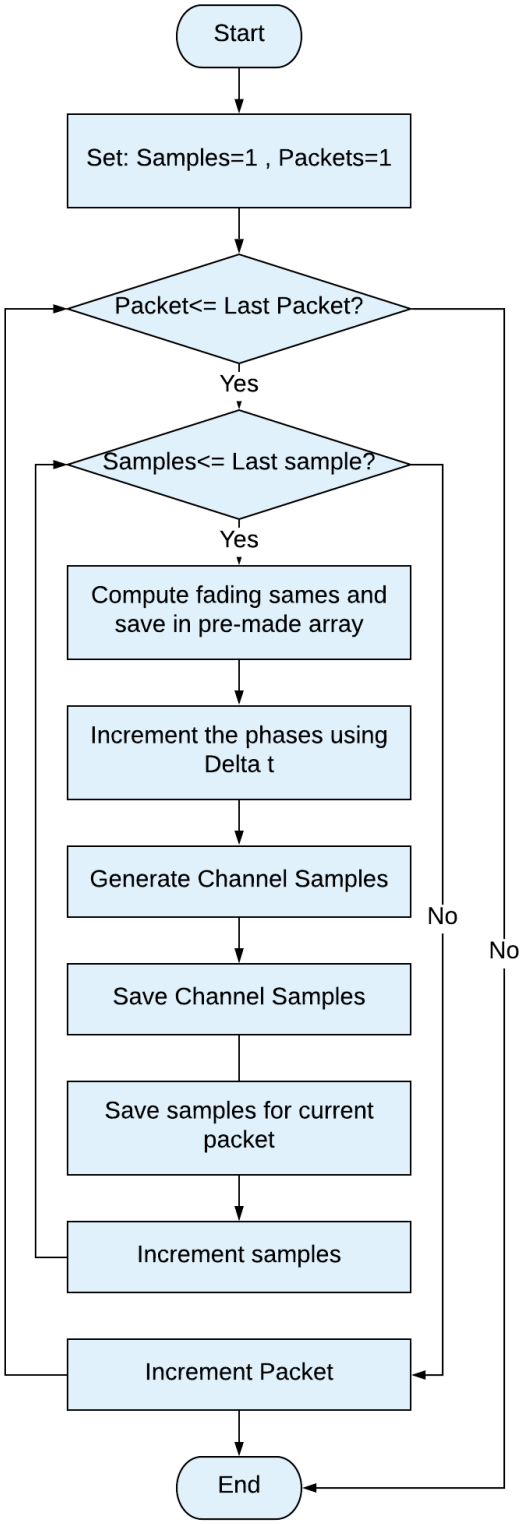

Figure 4.6: SOS sample Generating Function File

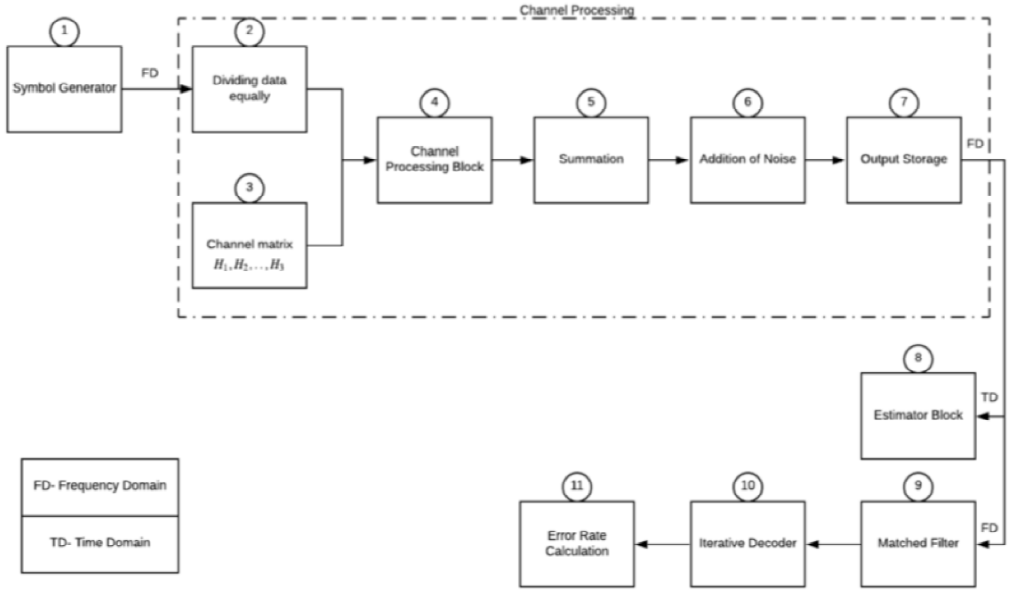

Figure 4.7: Simulink Estimator Model Flow Diagram

1. Here the data is mapped into QPSK symbols in frequency domain to form a data matrix, as described in section 2.8 while discussing Encoder. The design used for pilot sequences is based on [28]. Simulink Implementation of Encoder system is shown in figure 4.8.

2. Data matrix generated above is denoted by 'X' here. Now, this matrix is divided into 'k' parts, where 'k' is total number of sub-bands so that there exists one data matrix

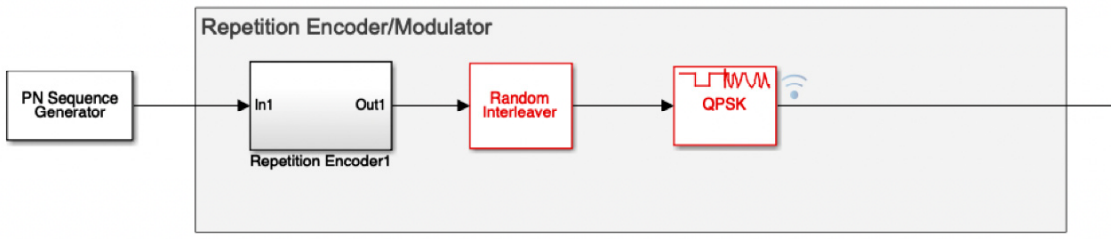

Figure 4.8: Simulink Implementation of Encoder System

for each channel matrix. These matrices are symbolised as $X_1, X_2, ..., X_3$ as used in equation 3.23.

3. This block contains all the channel matrices $H_1, H_2, ..., H_k$ to feed into channel processing block. Here, channels are in frequency domain.

4. This is where the data and channel are combined to give an output for each channel, which is represented as $Y_1, Y_2, ..., Y_k$.

5. All the outputs are summed in this block to give the output 'Y'.

6. White Gaussian Noise is added to the output here. Channel Processing blocks from figure 4.7 are implemented in Simulink as shown in figure 4.9 . The system shown in this figure is for three number of packets, i.e $k = 3$.

7. This block stores the output.

8. The estimator block uses Kalman filter which assumes the model is AR(1) (but in fact it is SOS or wide-band SOS model). As shown in Figure 4.10 it takes the AR(1) matrix which is basically a pilot signal, output signal from the wide-band channel, AR(1) noise matrix represented by A_1 and other parameters that provides any information regarding channel behaviour as discussed in section 2.9 and produces an estimated channel H_{est} or estimated output Y_{est}. These estimations are used to measure NMSE (Normalized Mean Square Error) or RE (Residual Error).

   NMSE (Normalized Mean Square error) with reference to the estimated channel matrix H_{est} and model generated channel matrix 'H' can be computed as,

$$\text{NMSE} = \frac{||H - H_{\text{est}}||^2}{||H||^2} \tag{4.1}$$

   The second method for calculating error is by measuring Residual Error (RE).

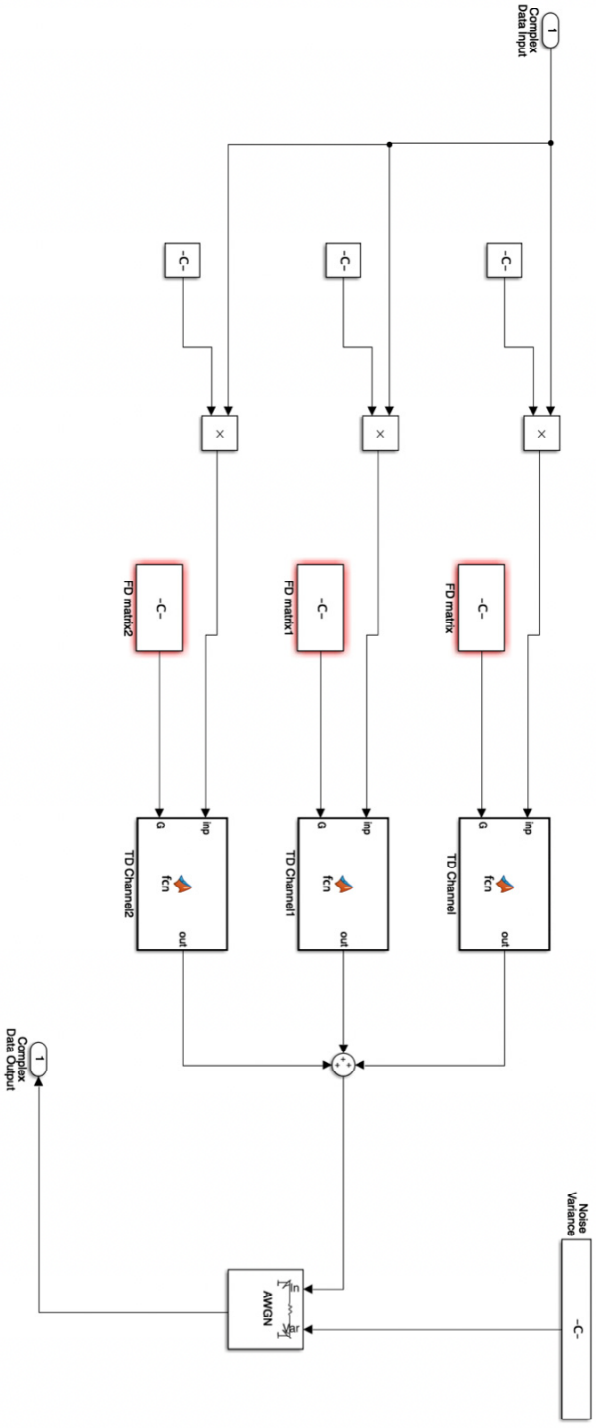

Figure 4.9: Simulink Implementation of the Channel Output Generation Block Using Wide-band Concept

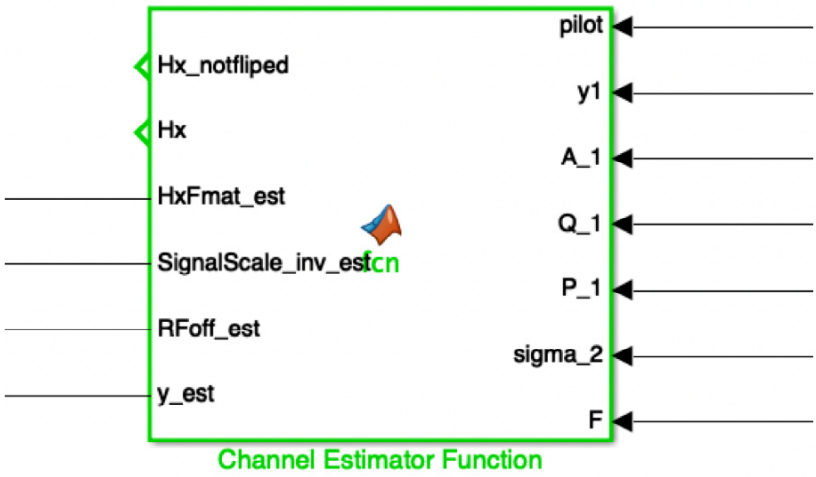

Figure 4.10: Simulink Implementation of Estimator Block

$$\mathrm{RE} = \frac{||Y - Y_{\mathrm{est}}||^2}{||Y||^2} \tag{4.2}$$

Here, Y_{est} can be known by,

$$Y_{\mathrm{est}} = H_{\mathrm{est}} P \tag{4.3}$$

In the experiments illustrated in next chapter, the designed simulink considers second approach, i.e computes residual error for estimation purpose.

9. In this block convolution of output signal takes place with appropriate Matched filter to revive the output to correctly decodable level, which was previously distorted due to white Gaussian noise. This is done as represented in equation 2.32 and 2.33

10. Figure 4.11 depicts the Simulink implementation of the decoder created on the basis of section 2.8.

11. Error rate calculator: The error rate calculator block determines the BER (Bit Error Rate) by comparing the sent data with the received data bits.

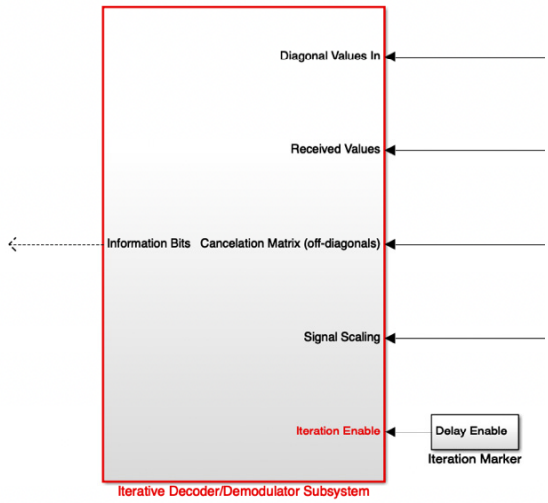

Figure 4.11: Simulink Implementation of Decoder System

4.4 Mathematical Representation of Simulink Model

The block diagram shown in Figure 4.7 holds true for narrow-band as well as wide-band simulink model. However, there are additions to the narrow-band model to design a wide-band channel model. This section briefs about the narrow-band case and explains the upgrades needed for wide-band simulink.

4.4.1 Narrow-band Simulink Model

In this model there exists only one channel matrix 'H' along with only one data set 'X'. It is to note that the 'H' matrix generated from the MATLAB program here is in time domain. However, the data set generated in simulink model is in frequency domain and hence is represented as $'X'_f$. Therefore, H matrix is also converted into frequency domain to get the output in following manner.

$$Y_f = H_f X_f \tag{4.4}$$

Further, the estimated output and the above derived output are compared in time domain while calculating mean square error.

4.4.2 Wide-band Simulink Model

Here, for a wide-band model we receive 'k' (where k is number of sub-bands) channel matrices in time domain. Each of them is converted into frequency domain. Although,the data matrices for each sub-band has same dimension as for narrow-band , data is available only at respective positions while rest all positions are set to zero. This is represented in equation 3.20. This scenario can be represented as,

$$Y_f = H_{1f}\begin{pmatrix} X_{1f} \\ 0 \\ 0 \\ \vdots \\ 0 \end{pmatrix} + H_{2f}\begin{pmatrix} 0 \\ \vdots \\ X_{2f} \\ \vdots \\ 0 \end{pmatrix} + H_{kf}\begin{pmatrix} 0 \\ 0 \\ 0 \\ \vdots \\ X_{kf} \end{pmatrix} \tag{4.5}$$

where, $H_{1f}, H_{2f}, ..., H_{kf}$ are channel matrices per packet in frequency domain, $X_{1f}, X_{2f}, ..., X_{kf}$ are data matrices per packet in frequency domain. Furthermore, for wide-band model the MSE is calculated in the same way by comparing estimated Y and derived Y in time domain.

4.5 Doppler Shift Parameter

Doppler shifts are the results of movement of transmitter or receiver in positive or negative direction of the signal. Generally, the Doppler shift frequencies being a function of arrival angles tend to be variable for multi-path channel with each path having its own arrival angle as shown in figure 2.3. Moreover, for a frequency dependent model (wide-band model) the Doppler shifts differs for every carrier frequency of each sub-band. That is,

there is different Doppler frequency for each path of every sub-band . Such Doppler shifts being complex cannot be practically compensated. Though wide-band channel model was designed as explained in above chapters but there was a scope of improving this model which could make it more realistic by considering packet and path specific Doppler shift. Thus, this section concentrates on addition of Doppler shift feature to designed wide-band model.

4.5.1 Doppler Shift Frequencies Calculation

Doppler shift frequencies can be computed as,

$$f_{ds} = f_{cj} \cos\theta_i \frac{V}{c} \tag{4.6}$$

where, V is velocity of moving transmitter, θ_i is angle of arrival for respective path from 1,2,...i, f_{cj} are the carrier frequencies for all the sub-bands, j=1,2,..k and c is the speed of sound underwater, i.e 1500m/s. Moreover, V in this model is kept as an input parameter which is measured during sea trial and varies according to the environmental factors of the experiment location.

To add the impact of Doppler shift in the channel model, the derived Doppler shift frequencies of each path are added to the Doppler spread frequencies for each path.

4.6 Wide-band AR(1) Model

The above demonstrated MATLAB + Simulink system helps to compare wide-band and narrow-band model with different set of experiments as performed in Chapter 5. It is observed that the Residual Error (RE) for narrow-band model is lower in comparison to wide-band, as the estimator uses AR(1) model designed with narrow-band concepts. The reason to use the same estimator for both the models is for creating a common reference

to generate NMSE or RE. However,for proper estimation purpose, in practice the AR(1) model should also be designed using wide-band theory,that is, using AR(1) model for every sub-band with its corresponding data, Doppler shift and Doppler spread parameters. AR(1) model used in this way is called as wide-band AR(1) model here. Hence, in this section a wide-band AR(1) model is conceptually described.

Figure 4.12 shows the flow of process undertaken to create the model wide-band. Initially, A_1 and Q_1 parameters which are dependent on Doppler spread and shifts are calculated for each sub-band as each sub-band has its own spread and shifts. Then in Simulink model, pilot signal is converted into frequency domain so it can be divided into 'k' sub-pilots, later, it is converted back to time-domain as the estimation process takes place in Time domain. Here, each sub-band has its corresponding estimator and they run in parallel. Thus, we have 'k' sub-estimates, each with different Doppler effects. These estimates are then combined in frequency domain and are transferred back to time domain for calculation of errors (NMSE or RE). Figure 4.13 represents the Simulink model for 3 sub-bands. Ultimately, this gives improved performance and shown in chapter 5.

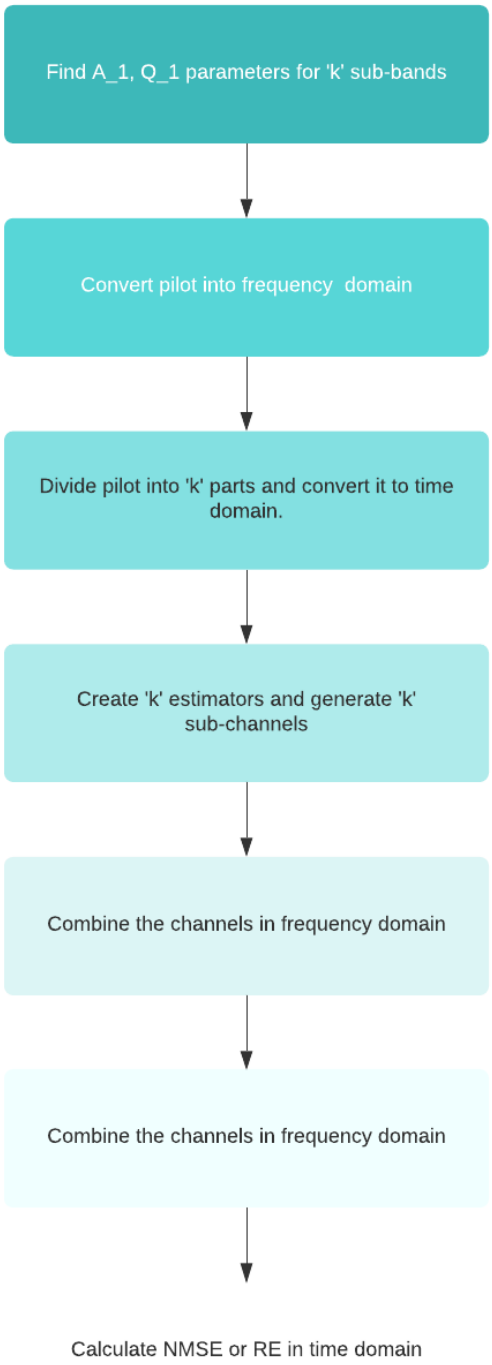

Figure 4.12: Block Diagram for AR(1) Wide-Band Process

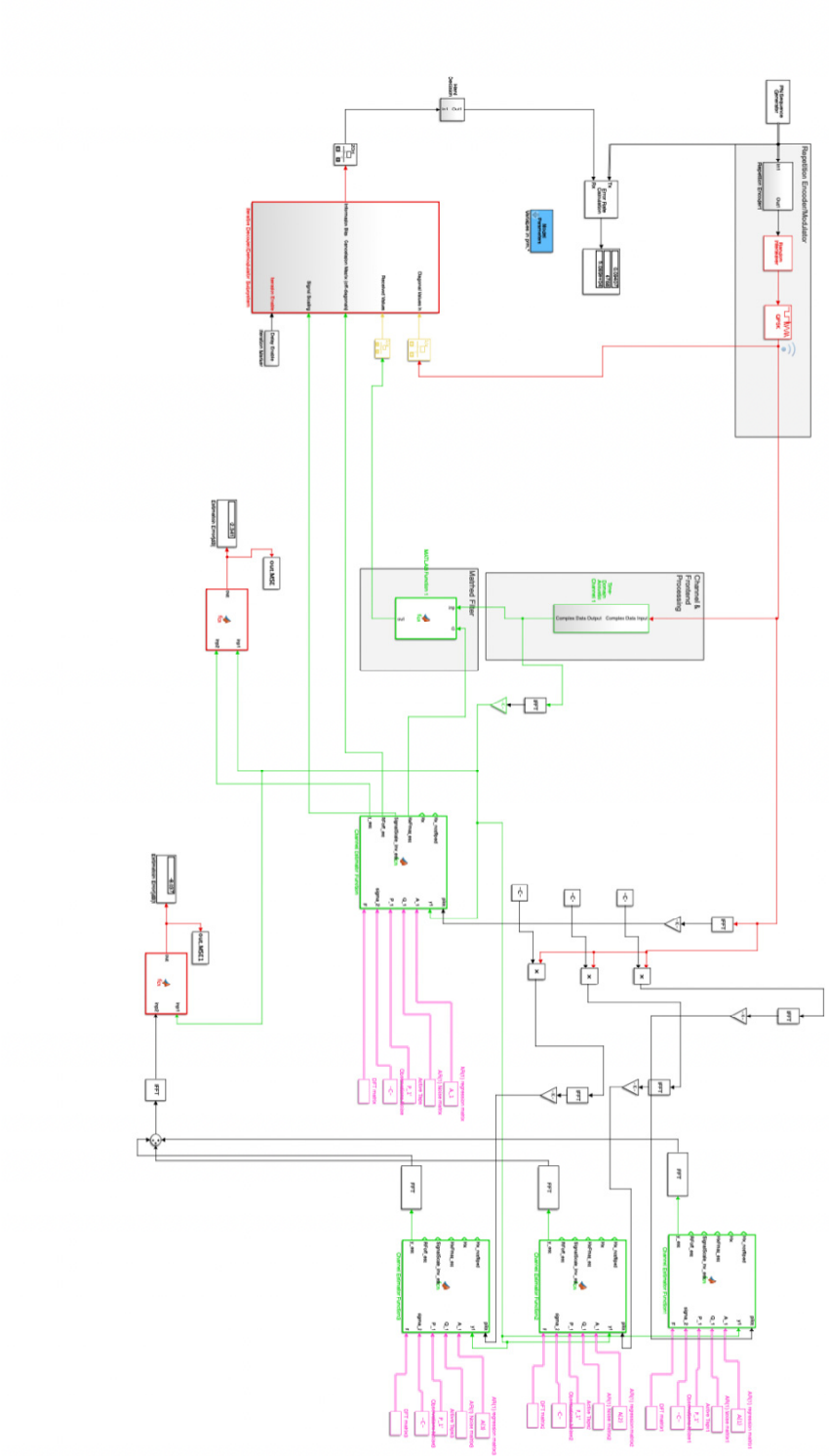

Figure 4.13: Simulink Implementation with wide-band AR(1) model for 3 sub-bands

Chapter 5

Results and Discussion

This chapter is divided into three sections. First section concentrates on comparing the Narrow-band model with wide-band and wide-band model with Doppler shifts by comparing their Residual Errors (RE) and BER (Bit Error Rate). Thus, proving the importance of frequency dependency and path specific Doppler. Moreover, this section discusses various cases such as, results of this model using wide-band system, consequences with varying Doppler shifts and also the variation in outcomes with changing number of sub-bands of the model. Where as, in second section some live data sets that are obtained from sea trials are studied to visualize the effect of change in Doppler spread with respect to varying bandwidth of a system. Lastly, in third section results with wide-band AR(1) model are studied by comparing the results obtained by using classic AR(1) model.

For all the experiments in first section the measuring parameters are the BER (Bit Error Rate) of the channels and RE (Residual Error) obtained form Simulink as explained in expression 4.2. Plots of RE and BER vs SNR (Signal to noise ratio) in decibel (dB) are generated so as to monitor the behavior of the channel at different SNR and how they vary with the change in factors that are to be observed. Moreover, tabular values are provided for each case for the clear picture of the same.

5.1 Experiments Using Designed Wide-Band Model

5.1.1 Experiment-1: Comparison of Narrow-Band and Wide-Band Model

These experiments focus on the difference in outcome when a wide-band model is used for the same underwater system instead of a narrow-band. Currently, the experiment is carried out for a system with smaller bandwidth as the narrow-band model is most accurate at smaller bandwidths. However, the experiments prove that wide-band model provides more realistic results for even smaller bandwidth in contrast to narrow-band model.

The SIMO system used in this experiment has a bandwidth of 320 Hz, carrier frequency taken as 1024. Doppler shifts velocity is considered to be as low as 0.5 m/s while introducing the shifts in the model. Doppler spread constant is 0.1 and the Simulink model is run for 100 iterations.

Narrow-Band Model Results

Table 5.1 displays the results of narrow-band model when used on the system stated above. As seen here, values of BER and RE are noted at SNR 10 dB,12 dB,14 dB,16 dB,18 dB and 20 dB. Figures 5.1 and 5.2 illustrates the same results of BER and RE for narrow-band model with red curves.

Wide-Band Model

In order, to use wide band model number of sub-bands are to be decided and given to the MATLAB file for a small bandwidth like 320, 3 sub-bands provide highly noticeable difference with very less complexity. This wide-band model includes the Doppler spread specific for frequencies in each sub-band, that is, Doppler shift differs with the changing carrier frequency of each sub-band as discussed in chapter 3. Table 5.2 provides the results using wide-band channel model for the system described for this experiment.

SNR (dB)	BER	RE
10	0.0033	-7.2467
12	0.000558	-9.3066
14	0.0001993	-11.3888
16	0.0000396	-13.4580
18	0	-15.6059
20	0	-17.7165

Table 5.1: BER and RE at variable SNR (dB) for narrow-band model

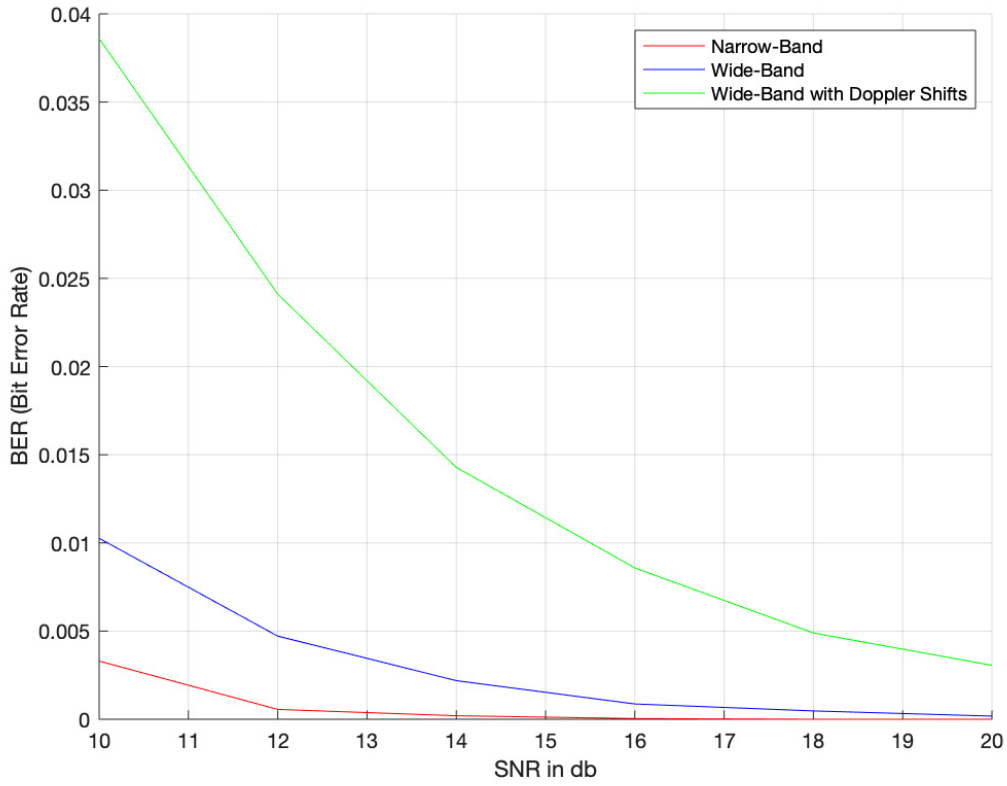

Figure 5.1: SNR (dB) vs BER for System with 320 Hz Bandwidth

Further, figure 5.1 portraits the nature of BER using wide-band model for different SNR (dB) values with blue curve. Whereas, figure 5.2 shows the residual error for wide-band model with blue cure as well.

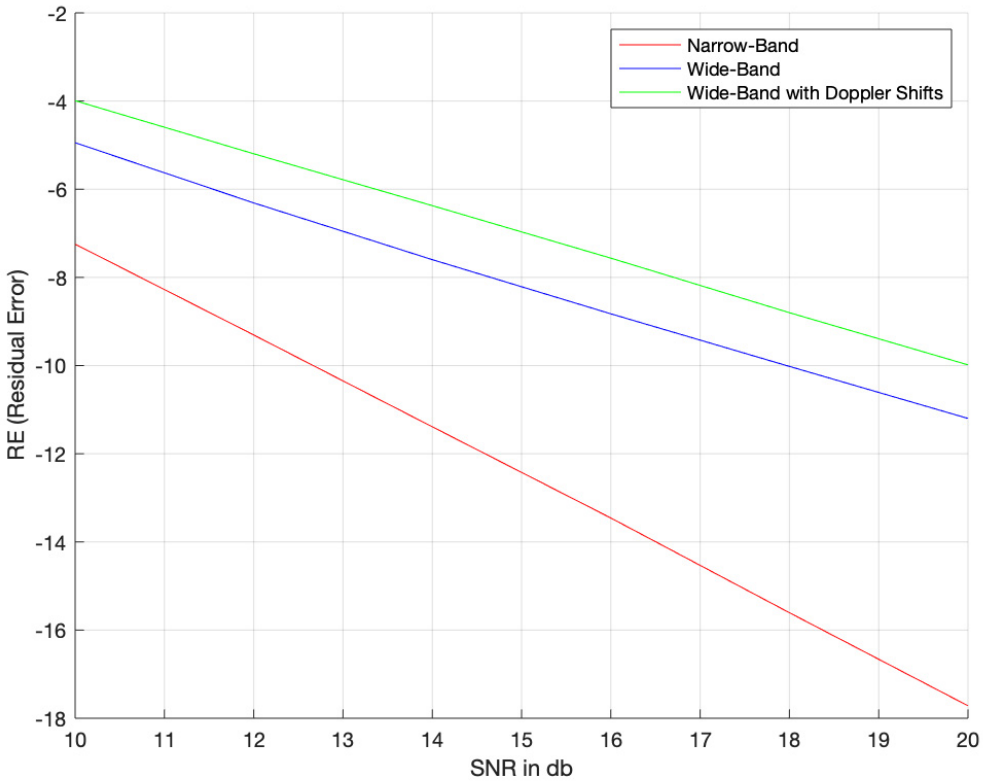

Figure 5.2: SNR (dB) vs RE for system with 320 Hz Bandwidth

SNR (dB)	BER	RE
10	0.01026	-4.9452
12	0.004715	-6.3107
14	0.00219	-7.5977
16	0.000868	-8.8262
18	0.0004733	-10.0192
20	0.0001776	-11.1992

Table 5.2: BER and RE at variable SNR (dB) for wide-band model

Wide-Band Model with Path Specific Doppler Spread

To make the wide-band model further accurate, the Doppler shifts are introduced in such a way that each path of each sub-band has its own Doppler shifts. Table 5.3 displays results

for such model. Moreover, figures 5.1 and 5.2 depicts these tabular results in graphical form with green lines.

SNR (dB)	BER	RE
10	0.0386	-3.9923
12	0.02411	-5.1957
14	0.01428	-6.3726
16	0.008582	-7.5637
18	0.004893	-8.8004
20	0.003058	-9.9837

Table 5.3: BER and RE at variable SNR (dB) for wide-band model with Doppler-shift

Discussion for Experiment-1

Taking into observation the results in figures 5.1 and 5.2 it can be neatly noticed that the narrow-band model is a model closer to estimated ideal model with less Bit Error Rate (BER) and hence having smaller Residual Error (RE), that signifies its resemblance to the estimated model.Firstly, discussing the BER for all the models, it can be noted from figure 5.1 that BER for each model decreases with increase in SNR (dB) as theoretically predicted. However, with further analysis it is clear that narrow band model shows that a channel has less Bit Error Rate (BER) when compared to wide-band model. This is due to lack of sensitivity of narrow-band model towards changing frequency in complete bandwidth. In contrast with this, wide-band model gives the BER considering the frequency changes in the bandwidth. Hence, large difference can be seen in the values when compared to narrow-band model. Further, when Doppler shifts corresponding to each path are introduced, more accurate picture of BER can be seen.

Residual error as expressed in 4.2 shows how the channel model coincides with an estimated model that is more theoretical and away from real life parameters. More the

negative value of RE or NMSE closer the model to estimated model. Considering figure 5.2 it is clear that the narrow band model highly coincides with the estimated model. Whereas, both the wide band model have elevated RE, which suggest that the Doppler parameters introduced have huge impact while underwater transmission which is not available while designing a system using narrow-band model in-turn providing less hints and scope for improvement of system design.

In a nutshell, it can be said that frequency specific Doppler spread and path and frequency dependent Doppler shifts have impacts that cannot be neglected in a channel model while providing a reliable tool for research for underwater system designer. Hence, rest all the experiments are carried out with the wide-band channel model that includes the Doppler shift parameter.

5.1.2 Experiment-2: Impact of Different Bandwidths on Models

Wide-band model as discussed before, being a frequency sensitive model provides detectable difference with the change in bandwidth. These results coincides with the consideration that as the bandwidth increases the channel becomes little more distorted. This is due to inclusion of more number of higher frequencies in the band along with lower. Therefore, the packets having higher carrier frequency in wide-band model will observe higher Doppler spread and shifts in comparison to the packets with lower carrier frequencies which in turn makes the final channel model a function of various carrier frequencies in each band and thus provides better accuracy. In contrast, in narrow-band model the sensitivity to bandwidth is not directly related to every changing frequency in the bandwidth. Hence, this model generates a response that changes insufficiently with respect to the change in bandwidth. Here, both the models are run for small to wide bandwidths and BER (Bit Error Rate) and RE (Residual Error) are noted to observe how the model behaves with varying frequency.

In this experiment all the parameters except bandwidth are kept the same for both the

models. That is, carrier frequency is set to 1024 Hz, number of packets/sub-bands set to 6, number of iterations to 100, Doppler coefficient (α) considers as 0.1 and the system is SIMO.

Results for Bandwidth = 500 Hz

SNR (dB)	BER	RE
10	0.00112	-7.0433
12	0.0001184	-9.0189
14	0.0000197	-10.9888
16	0	-12.9475
18	0	-14.8841
20	0	-16.7846

Table 5.4: BER and RE at variable SNR (dB) for narrow-band model at bandwidth 500Hz.

Table 5.4 and 5.5 represents value of BER and RE for narrow-band and wide-band model respectively. Also, figures 5.3 and 5.4 displays the off that narrow-band model holds when compared to wide-band for BER and RE respectively.

SNR (dB)	BER	RE
10	0.04418	-2.6162
12	0.04344	-3.8016
14	0.0306	-4.6824
16	0.02016	-5.5390
18	0.01592	-6.3972
20	0.008898	-7.1440

Table 5.5: BER and RE at variable SNR (dB) for wide-band model at bandwidth 500Hz.

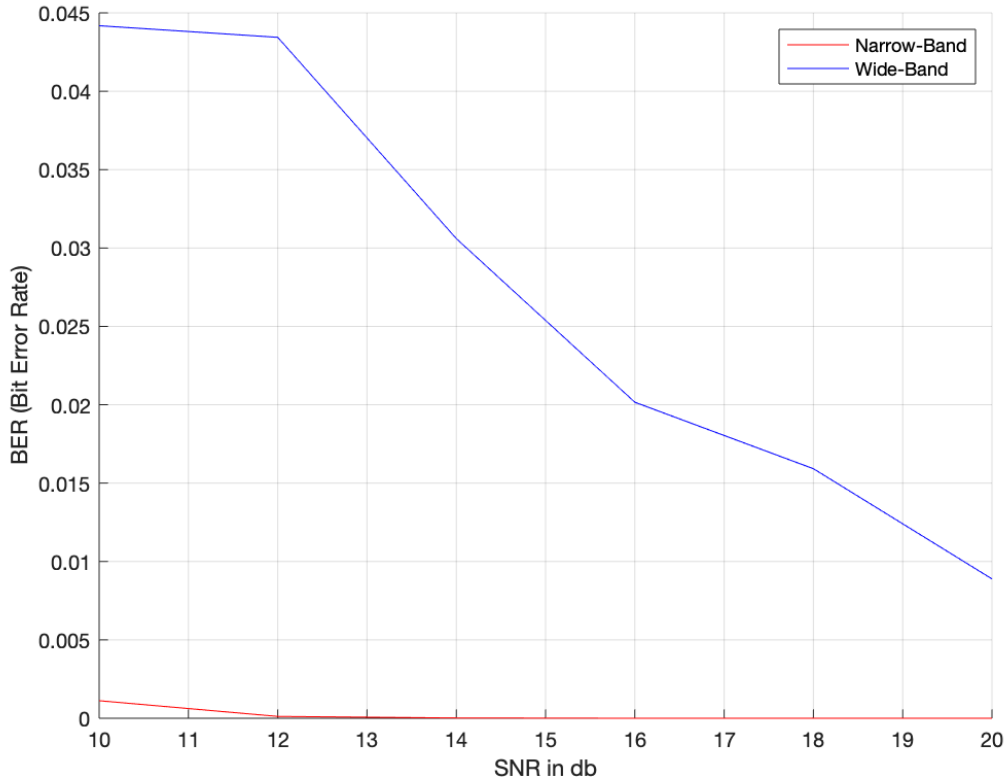

Figure 5.3: SNR (dB) vs BER for System with 500 HZ Bandwidth

As seen in figure 5.3 there is a non-negotiable difference in Bit Error Rates (BER) for narrow-band and wide-band model. Narrow-band model is subtle to the the changes in SNR (dB) where as, the wide-band model is more prompt. Moreover, such similar pattern of difference in values of RE can be seen in figure 5.4. This suggests that the narrow-band model has closer resemblance to estimated model and vice-versa. As noted for 20 dB SNR the narrow-band model has RE of -16.78 which signs that estimated and narrow-band model are remarkably alike. As the bandwidth increases this difference between narrow-band and wide-band model values can be seen increasing due to lack of frequency dependency of narrow-band model.

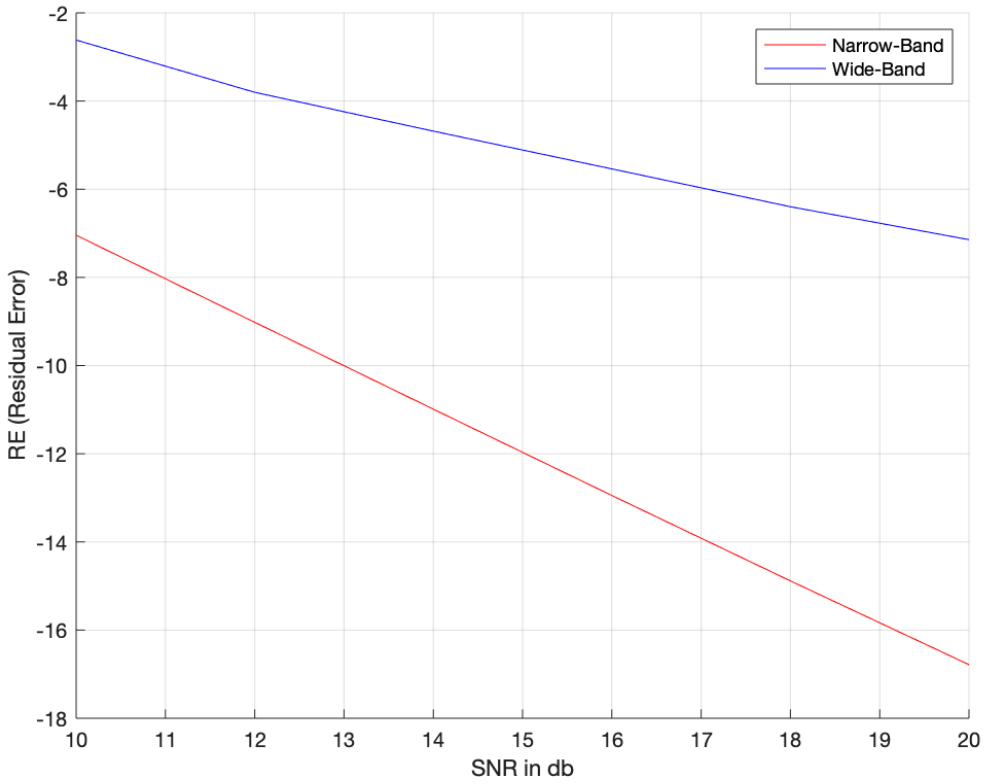

Figure 5.4: SNR (dB) vs RE for system with 500 Hz Bandwidth

Results for Bandwidth = 6000 Hz

Results for a wide-band underwater system with a bandwidth of 6000 Hz are presented in tables 5.6 and 5.7. Also, comparison of the results for both the models are illustrated in figures 5.5 and 5.6. According to these figures it can be noted that the difference between RE is noticeably higher at wider bandwidth than at 500 Hz bandwidth. Also, BER for both model has drastically different value, which shows a boost in accuracy with wide-band model.

Results for Bandwidth = 15,000 Hz

Figures and tables in this subsection represents the same comparison for even higher bandwidth of 15,000 Hz. Figure 5.7 and 5.8 depicts BER and RE comparison for both the

SNR (dB)	BER	RE
10	0.02107	-7.1678
12	0.01385	-8.9902
14	0.009332	-10.7171
16	0.005938	-12.3152
18	0.004143	-13.7510
20	0.003413	-14.9984

Table 5.6: BER and RE at variable SNR (dB) for narrow-band model at bandwidth 6000 Hz.

SNR (dB)	BER	RE
10	0.1245	-1.9343
12	0.1165	-2.4186
14	0.1095	-2.7614
16	0.1045	-3.0036
18	0.09985	-3.1800
20	0.09535	-3.3181

Table 5.7: BER and RE at variable SNR (dB) for wide-band model at bandwidth 6000 Hz.

models respectively. Noting from table 5.8 and 5.6 it is clear that there is negligible difference in BER for higher bandwidth of 15,000 Hz when compared to 6000 Hz bandwidth. Same holds true for values of RE. This proves deteriorated performance of narrow-band model for higher bandwidths.

Discussion

As seen from all the results for different bandwidths it is evident that there is noteworthy difference between narrow-band and wide-band model. Moreover, as the bandwidth increases this contradiction of both models keeps on increasing. Considering values in table

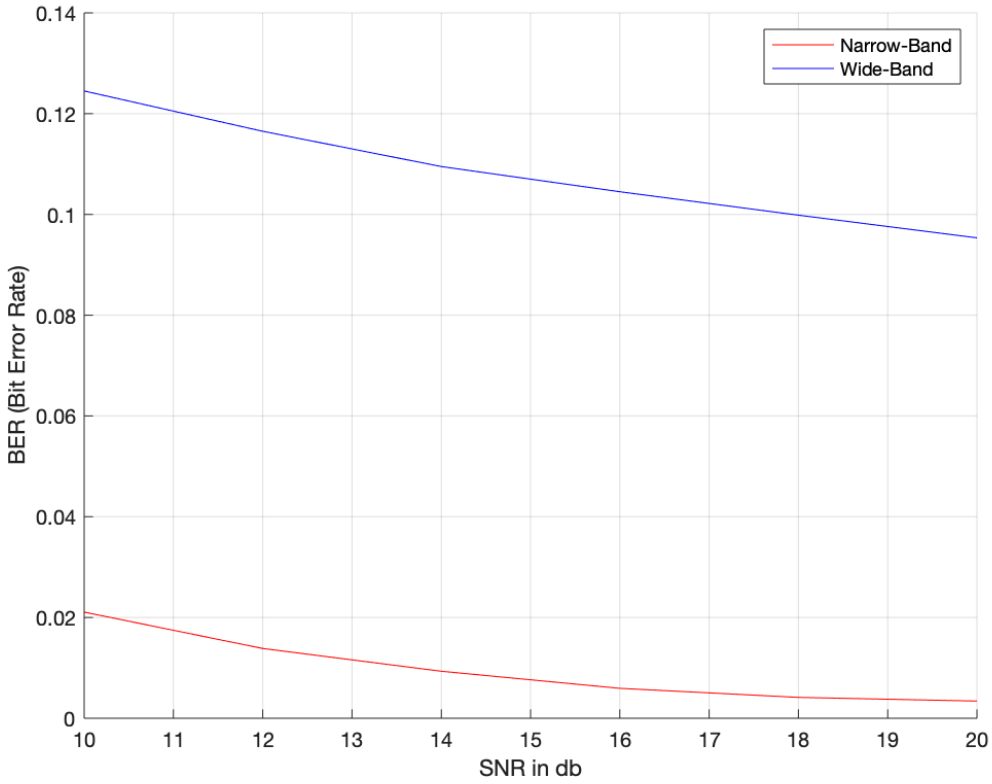

Figure 5.5: SNR (dB) vs BER for System with 6000 HZ Bandwidth

SNR (dB)	BER	RE
10	0.02569	-7.1255
12	0.01671	-8.9757
14	0.01134	-10.7396
16	0.008266	-12.3825
18	0.005958	-13.8653
20	0.004893	-14.8761

Table 5.8: BER and RE at variable SNR (dB) for narrow-band model at bandwidth 15,000 Hz.

5.4, 5.6 and 5.8 it is clear that the values of RE and BER shows trivial difference for varying bandwidth. However, unlike narrow-band model wide-band model is highly susceptible to

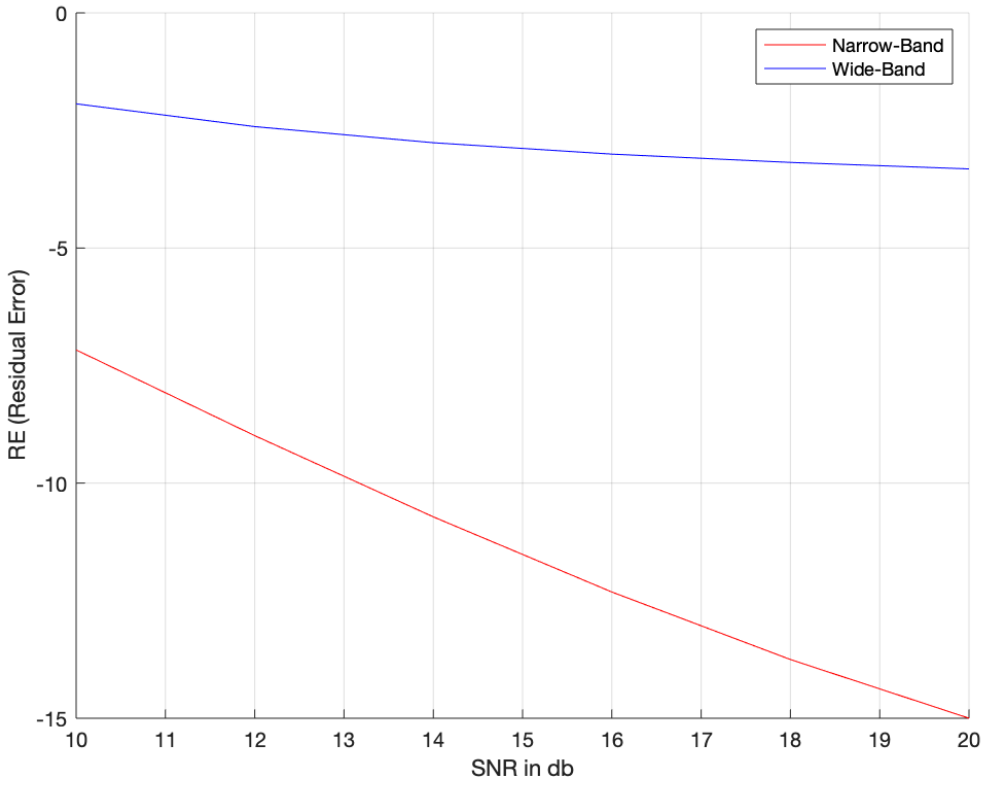

Figure 5.6: SNR (dB) vs RE for system with 6000 Hz Bandwidth

SNR (dB)	BER	RE
10	0.166	-1.4339
12	0.1592	-1.8703
14	0.1537	-2.1714
16	0.1498	-2.3749
18	0.1475	-2.5118
20	0.1453	-2.6055

Table 5.9: BER and RE at variable SNR (dB) for wide-band model at bandwidth 15,000 Hz.

bandwidth differences. To present this in a pictorial manner figure 5.11, 5.12 and 5.9, 5.10 where the former set of figure stands for wide-model comparing its RE's and BER's at 500

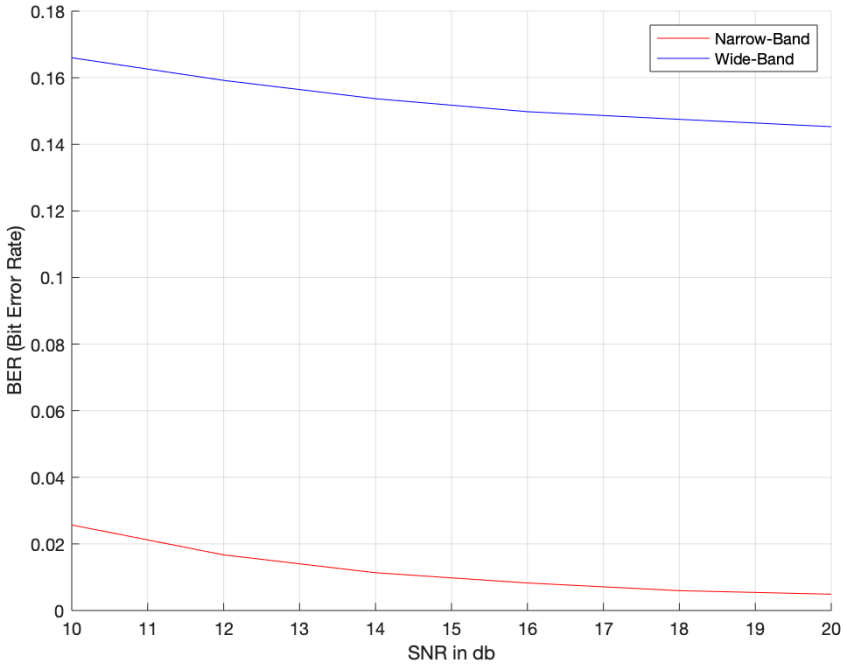

Figure 5.7: SNR (dB) vs BER for System with 15 kHZ Bandwidth

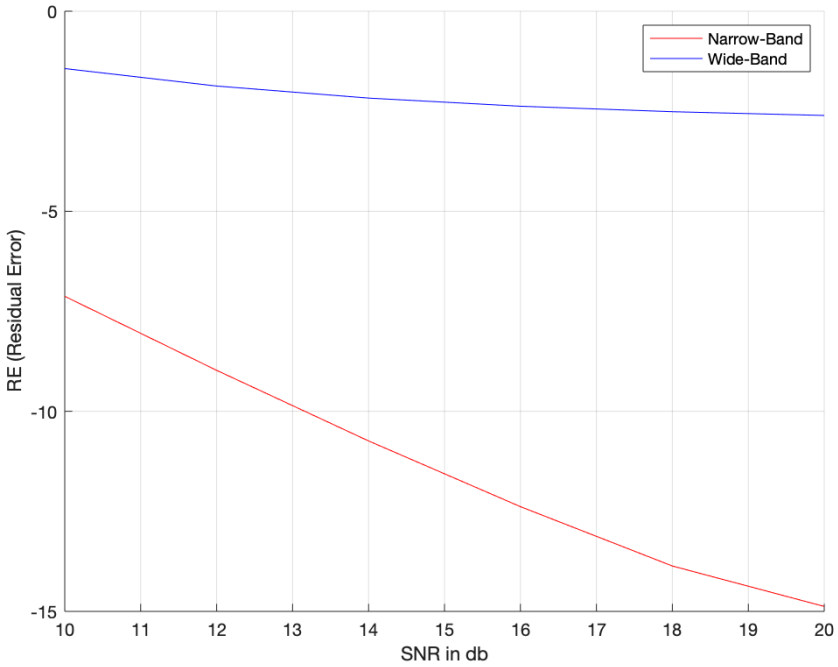

Figure 5.8: SNR (dB) vs RE for system with 15 kHz Bandwidth

Hz and 6000 Hz and 15,000 Hz bandwidth and the latter set of figures depicts the same for narrow-band model. The accuracy of narrow-band model fades further for wider bandwidths which is not the case with wide-band channel. Moreover, increasing the number of packets as the bandwidth increases the wide-band model produces more factual results. However, for fair comparison of the models number of packets were kept same for each trial run. This experiment thus proves the name apt for the wide-band model.

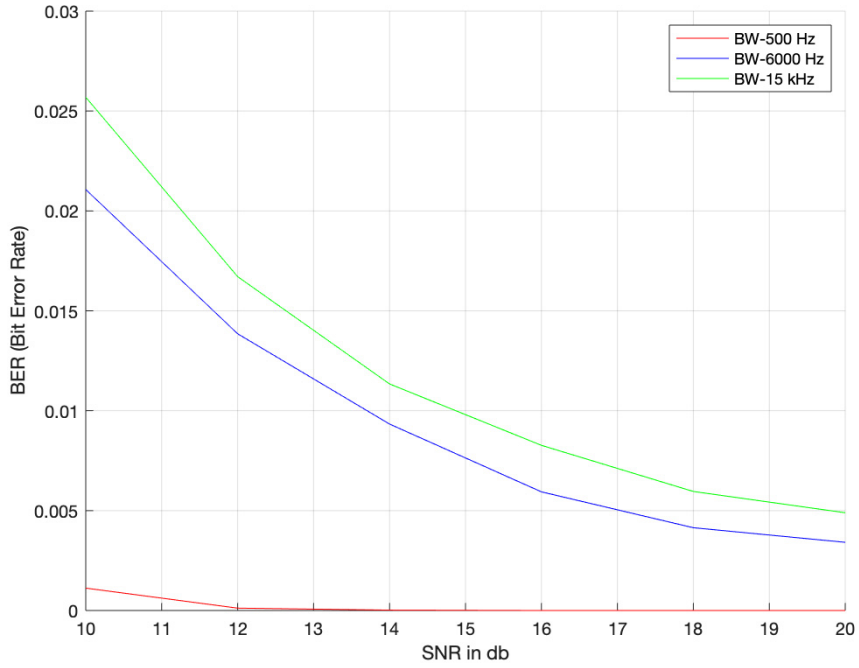

Figure 5.9: SNR (dB) vs BER for Narrow-Band model at different Bandwidths

5.1.3 Experiment-3:Impact of Number of Packets/ Sub-bands

Wide-band channel as explained in chapter 3 divides the bandwidth into 'k' sub-bands for precise results. As the bandwidth increase, proportionally number of sub-bands should be increase to maintain the precision. Moreover, higher the number of packets better the accuracy of channel model. This experiment is for a system with carrier frequency of 1024 Hz, Bandwidth of 3000 Hz with $\alpha = 0.1$ and 100 iterations. Number of packets used to get

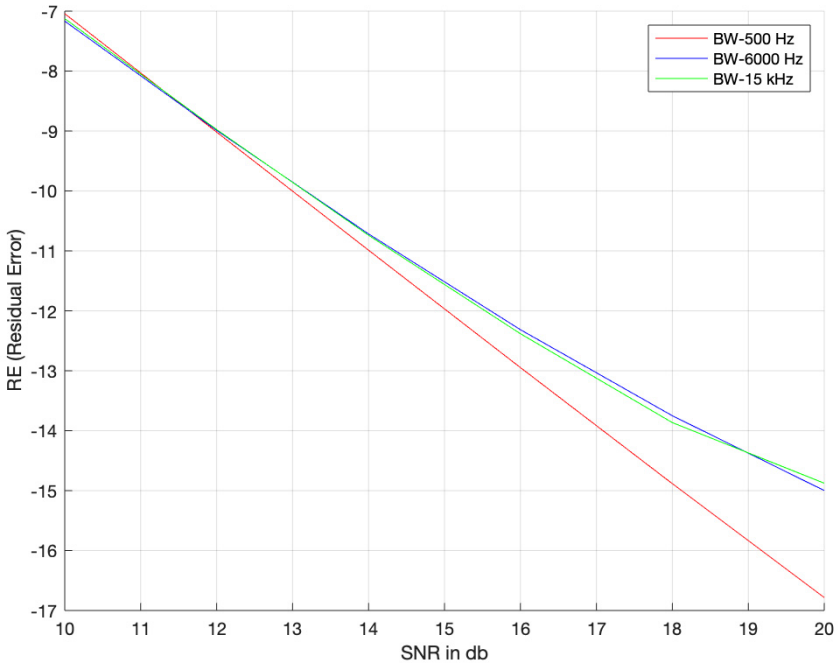

Figure 5.10: SNR (dB) vs RE for Narrow-Band model at Different Bandwidths

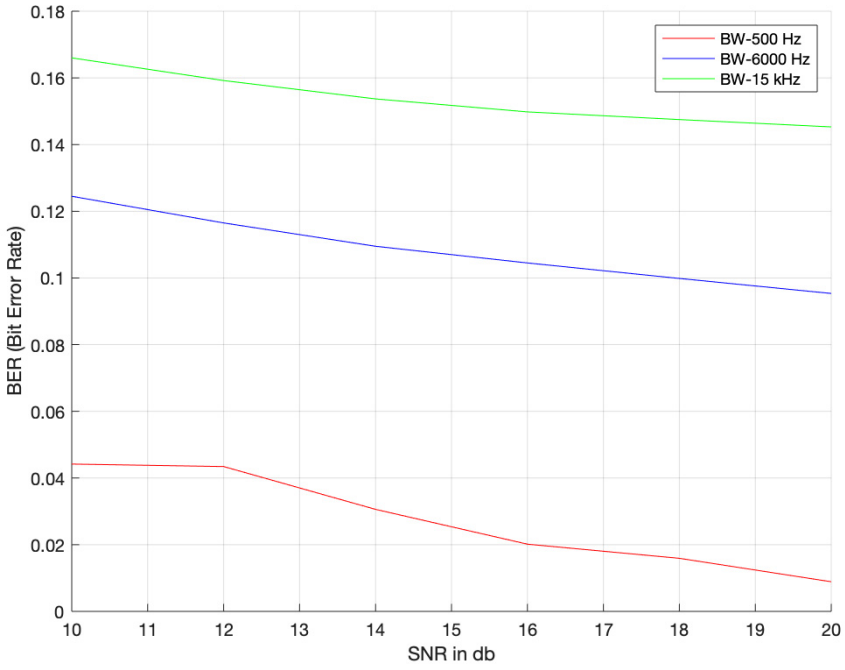

Figure 5.11: SNR (dB) vs BER for Wide-Band model at different Bandwidths

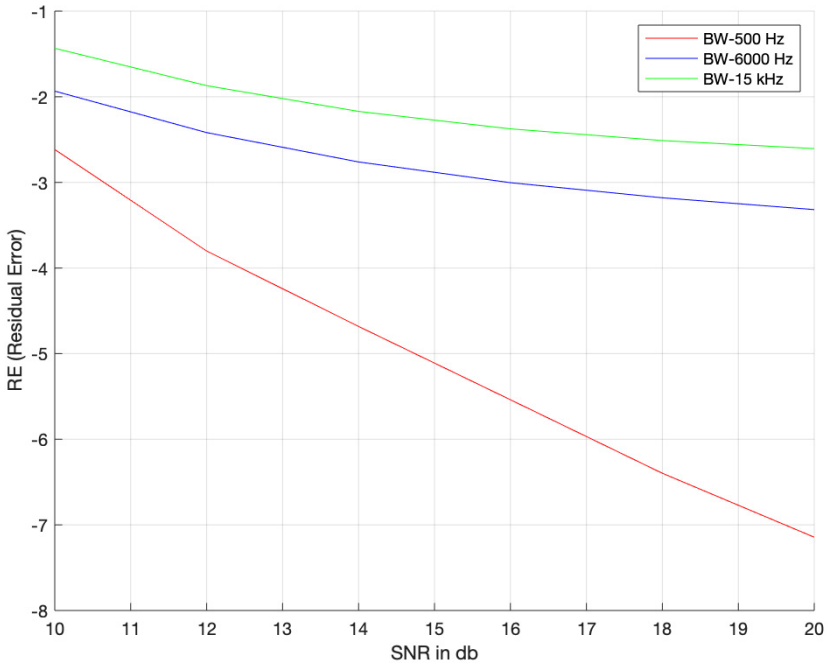

Figure 5.12: SNR (dB) vs RE for Wide-Band model at Different Bandwidths

a channel using model are 3,6 and 9. Table 5.10, 5.11 and 5.12 hold the values for BER and RE for each case. Figures 5.13 and 5.14 represent the improvement in the channel model performance with increasing packets.

SNR (dB)	BER	RE
10	0.0901	-3.2710
12	0.07588	-3.9851
14	0.06465	-4.5414
16	0.05556	-4.9792
18	0.0481	-5.3334
20	0.04321	-5.6321

Table 5.10: BER and RE at variable SNR (dB) for 3 packets

SNR (dB)	BER	RE
10	0.1052	-2.1685
12	0.09359	-2.7118
14	0.08353	-3.1215
16	0.7641	-3.4393
18	0.07012	-3.6999
20	0.06341	-3.9296

Table 5.11: BER and RE at variable SNR (dB) for 6 packets

SNR (dB)	BER	RE
10	0.12	-1.6813
12	0.1097	-2.1572
14	0.09971	-2.5058
16	0.09121	-2.7669
18	0.08306	-2.9729
20	0.07582	-3.1490

Table 5.12: BER and RE at variable SNR (dB) for 9 packets

Discussion

Figure 5.14 and 5.13 justifies the role of number of packets in accuracy. Higher the number of packets, response is more reliable. Ideally a most accurate model would have a separate Doppler shift effect for each frequency. However, this is not feasible practically due to complexity of the concept. Though this model does not generate a separate Doppler dependent channel for each frequency of bandwidth but as discussed in chapter 4 it proves sub-bands that has near by frequencies in which the spread would different in small amount to give better results and smaller the band less would be variation in frequency and hence it works with higher accuracy. Also, number of packets should be decided by user keeping

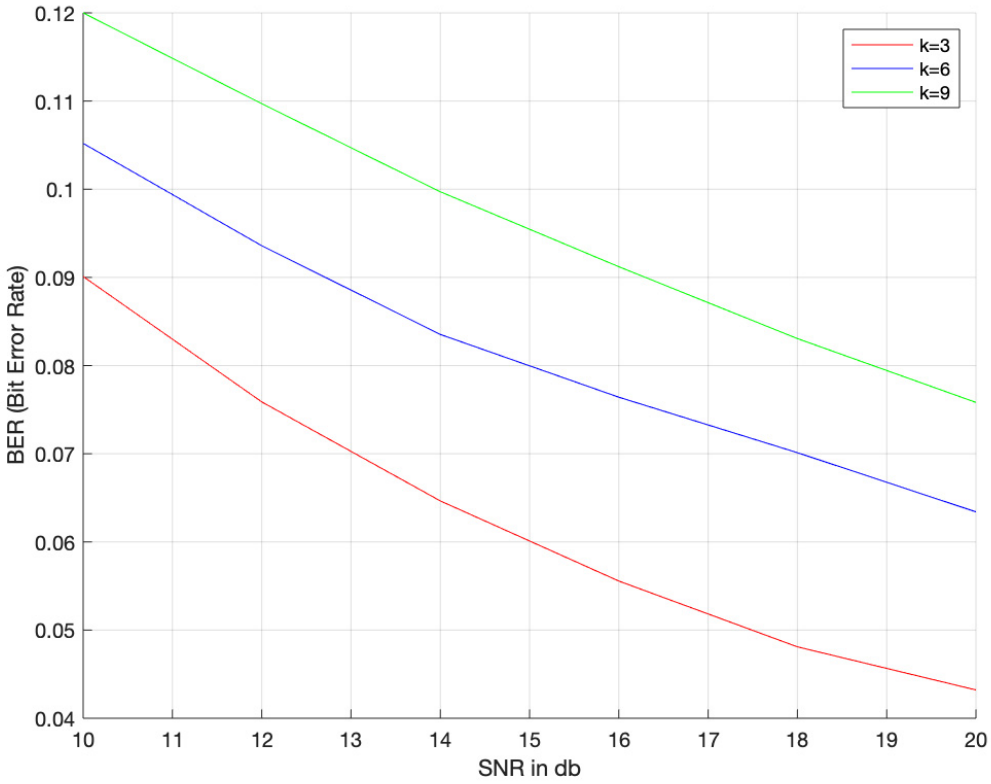

Figure 5.13: SNR (dB) vs BER for different number of packets

in mind the bandwidth.

5.1.4 Experiment4: Impact of Variation of velocity of Transmitter on Doppler Shifts

Doppler shifts are function of velocity of either moving transmitter or receiver or both as described in expression 2.1. As the velocity changes the shifts are varied. This is verified in this section by comparing RE and BER for a velocity of transmitter as 1 m/s and 2 m/s. While velocity is an input parameter in this model, the narrow band model is not sensitive to any Doppler frequencies generated due to varying velocity, posing a reason for generalized model. This experiment is carried out for a system with a bandwidth of 2500 Hz and carrier

frequency of 1024. Table5.13 and 5.14 holds the data represented in figure 5.15 and 5.16.

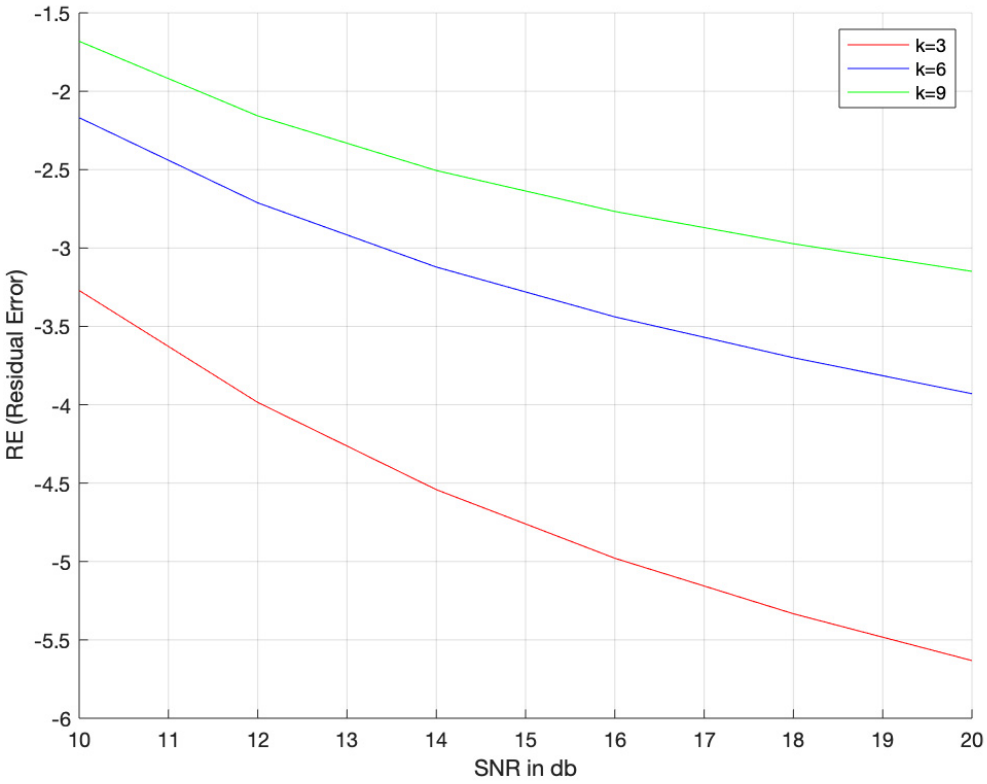

Figure 5.14: SNR (dB) vs RE for different number of packets

SNR (dB)	BER	RE
10	0.07173	-3.2317
12	0.05674	-4.0339
14	0.04443	-4.7304
16	0.0346	-5.3567
18	0.02726	-5.5390
20	0.02212	-6.4769

Table 5.13: BER and SNR (dB) at variable SNR (dB) Transmitter Velocity of 1 m/s

Discussion

The values in tables 5.13 and 5.14 shows a vast difference in BER and considerate amount of difference in RE. Hence, this proves to be an important parameter to be incorporated

SNR (dB)	BER	RE
10	0.1519	-1.3080
12	0.1287	-2.9584
14	0.1039	-3.5189
16	0.08126	-4.0326
18	0.06011	-4.5313
20	0.04228	-5.0360

Table 5.14: BER and RE at variable SNR (dB) Transmitter Velocity of 2 m/s

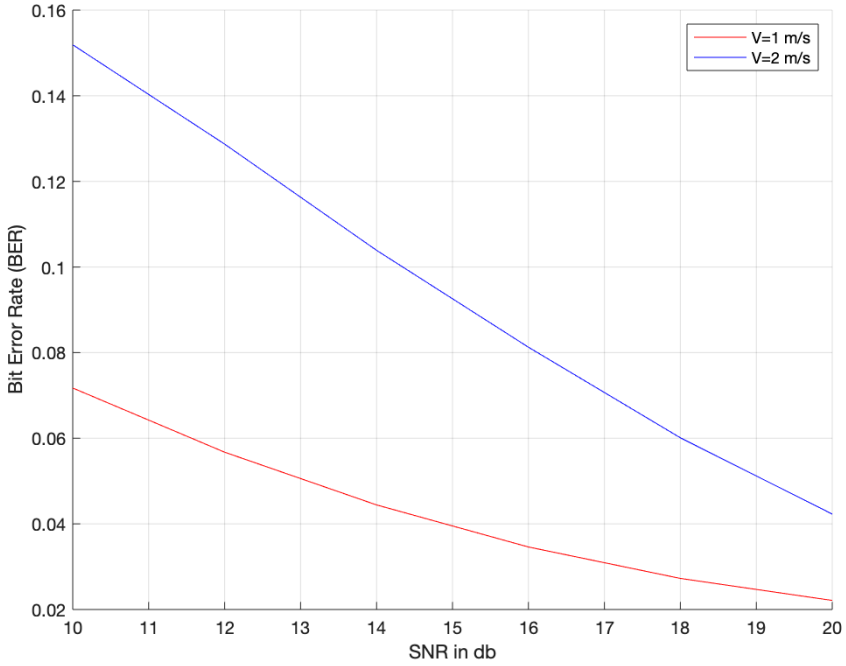

Figure 5.15: SNR (dB) vs BER for variable Transmitter Velocities

in a model. Moreover, though average shifts can be compensated manually as done for narrow-band model but, shifts that are introduced due to different arrival angle are hard to compensated and can be studied further.

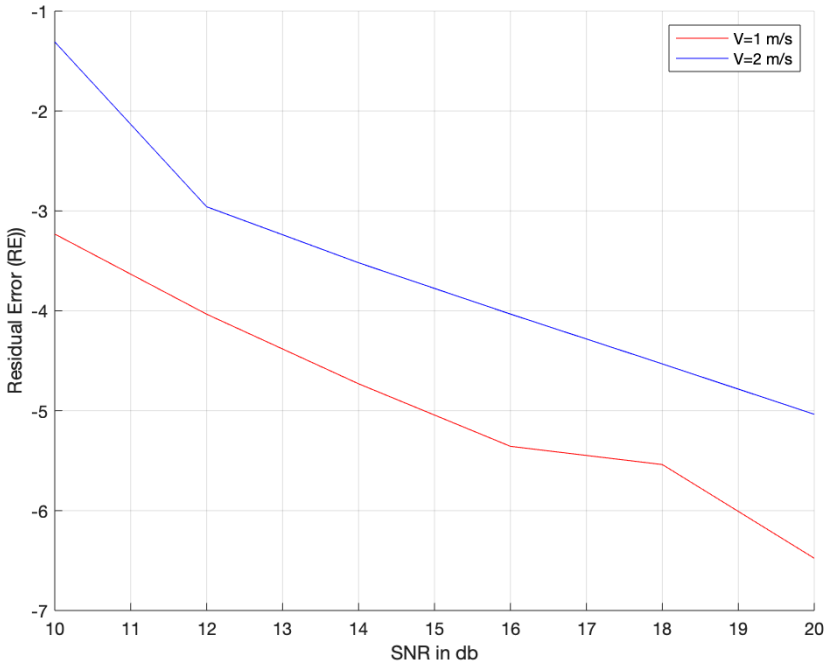

Figure 5.16: SNR (dB) vs RE for variable Transmitter Velocities

5.2 Study of Sea Trial Results

In this section real life data obtained from sea-trials done in August'2019 is examined in order to see how the Doppler spread is proportional to the bandwidth of the system. This experiments were carried out in Peggys Cove, Nova Scotia waters, Canada in considerably calm weather conditions. The setup for this experiments included a transmitter system dropped at a depth of 30 meters and a receiver system having five hydrophone array with a distance of 40 cm between them submerged at a depth of 30 meters as well. The transmission distance for the sound files used here was 1 km. The files plotted in figure 5.18 are pilots only.

The pilot structure used here can be explained as shown in figure 5.17. As seen the this figure, one pilot signal constitutes of 64 preambles and such 16 pilots are combined to make a signal.

Lower and Higher bandwidth signals used here has a bandwidth of 2000 Hz and 6000

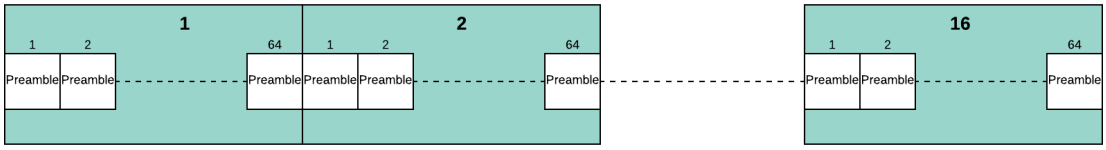

Figure 5.17: Pilot Structure Used for Sea Trial Signals

Hz respectively, carrier frequency is 25 kHz and sampling frequency is 96 kHz. Following plot depicts the Doppler spread for both the cases.

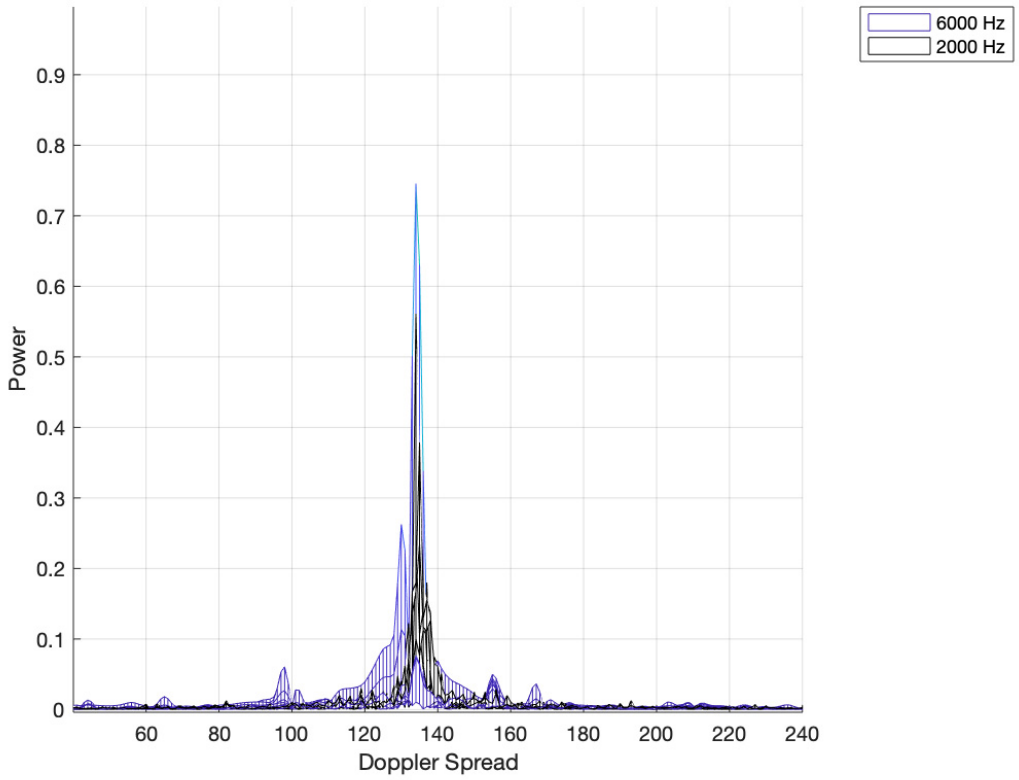

Figure 5.18: Doppler Spread for 2000 Hz and 6000 Hz Signal plotted using data of August'2019, Nova Scotia Waters.

Discussion

As seen in the figure 5.18 the black data represents 2 kHZ signal and data in blue represents 6 kHz signal. The x-axis shows the Doppler spread and each box along x-axis equals to

5 Hz, where as, Y-axis represents power of the taps. It should be noted that the figure is plotted for only the samples that holds signal and rest frequency axis is trimmed out of the picture. Hence, the Doppler spread across the X-axis is to be observed relative to each other rather than considering the frequency values over the axis. Thus, from the plot in figure 5.18 that the spread for the 6000 Hz signal is higher than the spread for 2000 Hz signal, which conveys the significance and need of a wide-band model.

5.3 Results Using Wide-Band AR(1) Model in Estimator

As described in section 4.6 for using the wide-band model and for measuring the correct error the estimator should have a wide-band AR(1) model. In this section the AR(1) wide-band model is utilized in estimator for experiments with two signals are carried out, one with the bandwidth of 6000 Hz and other with 15 kHz. Carrier frequency here is 1024, Doppler shift velocity is 2 m/s, three sub-bands are used to make it a wide-band model.

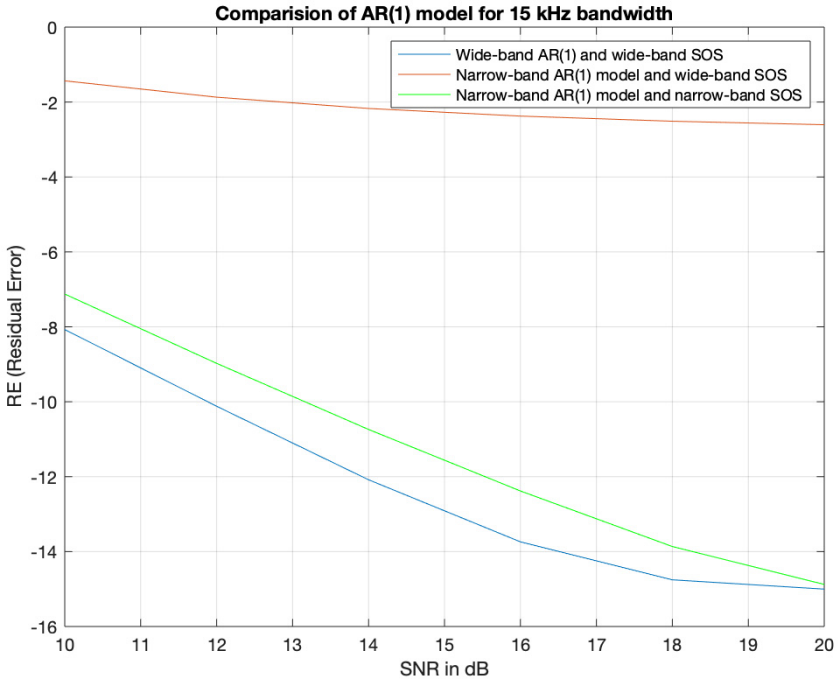

Figure 5.19: SNR (dB) vs RE for testing AR(1) model on 15 kHz bandwidth

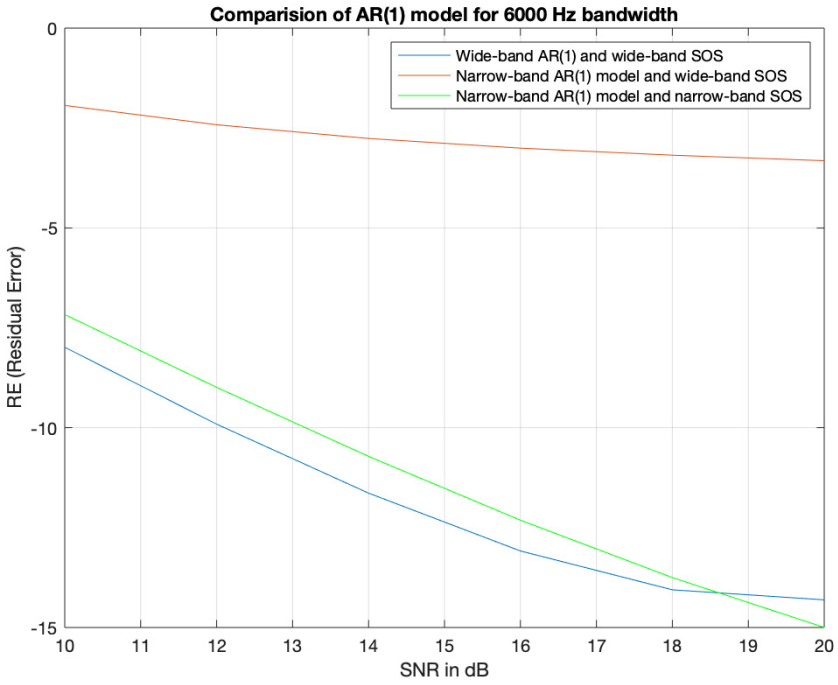

Figure 5.20: SNR (dB) vs RE for testing AR(1) model on 6 kHz bandwidth

Figure 5.19 and 5.20 displays results for the signal with 15kHz and 6000 Hz bandwidth respectively. Here, the Residual error obtained while using narrow-band AR(1) model in estimator is compared with the Residual Error (RE) observed by utilizing wide-band based AR(1) model. It is seen that there is a significant decrease in RE bringing the AR(1) model more closer to the SOS model. Also, these results are compared to the RE obtained while using narrow-band AR(1) model to estimate and find error for narrow-band SOS model. It can be noted from this, that when wide-band based AR(1) model is used to derive RE for a wide-band SOS model it gives as less error as the error when narrow-band AR(1)model was used to find RE for narrow-band model. This proves that the AR(1) wide-band model has achieved the similarity to the SOS model as much as the narrow-band AR(1) model held for narrow-band SOS model.

Chapter 6

Conclusions and Future Work

6.1 Conclusions

1. In this thesis, we observed how the performance of a Sum-of-Sinusoids (SOS) based channel modeling software can be improved and how the model can be made available for all bandwidths by crafting a wide-band model that approaches frequency dependency of the channel such that, there is distinct Doppler spread instead of generalized Doppler spread. Also, we studied how the narrow-band and wide-band model behave at different bandwidth, finally proving the necessity and importance of wide-band/frequency dependent model.

2. It can also be concluded that, as the bandwidth increases, frequency independent model produces results that are more of a hypothesis, this makes it crucial to utilize frequency dependent model to get confident results.

3. This literature proves that it is a necessity to include path specific Doppler shifts as the common part of the Doppler shifts can be compensated but not the part caused due difference in arrival angles, which is different for each path. Moreover, this thesis has introduced a model not only with path specific shifts but also making the shifts frequency dependent to provide reliable results closer to real life scenario.

4. As the bandwidth increases the number of sub-bands are required to be increased for continuing the accuracy of the model. However, as seen in experiments model holds an affordable complexity even for higher bandwidths.

5. To support the conclusions, live data is studied which proves that there is variation in Doppler spread with respect to carrier frequency. Thus, it is crucial to have a model that considers this impact to advance the current models along with creating receiver and estimators that adopts a wide-band model.

6.2 Future Work

1. There is scope of designing a less complex and convenient estimator inculcating wide-band theory based AR(1) model that can be easily used for larger number of sub-bands.

2. Not just Estimator but also the complete receiver system can be designed that fits wide-band or frequency dependent concept.

3. Research can be done on hypothesis of a model that has a different Doppler spread for every frequency of bandwidth with a complexity that can be handled in order to provide a immensely accurate tool for system designing research for underwater communication.

Bibliography

[1] C.Schlegel, *Ultra Maritime Digital Communication Centre 5-year Report*. 2017.

[2] J. Peterson and M. Porter, "Ray/beam tracing for modeling the effects of ocean and platform dynamics," *Oceanic Engineering, IEEE Journal of*, vol. 38, pp. 655–665, 10 2013.

[3] G. Brooke, D. Thomson, and G. Ebbeson, "Pecan a canadian parabolic equation model for underwater sound propagation," *Journal of Computational Acoustics - J COMPUT ACOUST*, vol. 9, pp. 69–100, 03 2001.

[4] Parastoo Qarabaqi and Milica Stojanovic, "Stastical characterization and computationally efficient modeling of a class of underwater acoustic communication channels," *IEEE JOURNAL OF OCEAN ENGINEERING*, vol. 38, pp. 701–717, September 2013.

[5] P. A. Baxley, H. Bucker, V. K. Mcdonald, J. A. Rice, and M. B. Porter, "251 shallow-water acoustic communications channel modeling using three-dimensional gaussian beams," 2019.

[6] X. Wang, R. Jiang, W. Wang, and Q. Chen, "Channel modelling and estimation for shallow underwater acoustic ofdm communication via simulation platform.," *MDPI journals*, p. 447, 09 2019.

[7] P.-J. Bouvet and A. Loussert, "Capacity analysis of underwater acoustic mimo communications," pp. 1 – 8, 06 2010.

[8] A. Radosevic, D. Fertonani, T. Duman, J. Proakis, and M. Stojanovic, "Capacity of mimo systems in shallow water acoustic channels," pp. 2164 – 2168, 12 2010.

[9] D. Truhachev, C. Schlegel, M. Bashir, and J.-F. Bousquet, "Modeling of underwater acoustic channels for communication system testing," pp. 1–8, 10 2018.

[10] P. Walree, T. Jenserud, and M. Smedsrud, "A discrete-time channel simulator driven by measured scattering functions," *Selected Areas in Communications, IEEE Journal on*, vol. 26, pp. 1628 – 1637, 01 2009.

[11] F.-X.Socheleau, C.Laot, and J.-M.Passerieux, "Stochastic replay of non-wssus underwarter acoustic communication channels recorded at sea," *IEEE Transactions on Signal Processing*, vol. 59, pp. 4838–4849, October 2011.

[12] Ahmad, A.-M(Abdel-Mehsen), M Barbeau, Garcia-Alfaro, J. (Joaquin), Kassem, J. (Jamil), E. Kranakis, Porretta, and S.(Steven), "Doppler effect in the underwater

acoustic ultra low frequency band," *ADHOCNETS 2017: 9th International Conference on Ad Hoc Networks, Niagara Falls, Canada.*, pp. 3–12, September 2017.

[13] Xavier Lurton, *An Introduction to Underwater Acoustics: Principles and Applications.* Springer, 2002.

[14] X. Chen, Y. Pan, Y. Wu, and G. Zheng, "Research on doppler spread of multipath channel in subway tunnel," pp. 56–59, 03 2015.

[15] P. Van Walree, T.Jenserud, and R.Otnes, "Stretched-exponential doppler spectra in underwater acoustic communication channels," *The Journal of Acoustic Society of America*, vol. 128, November 2010.

[16] D.Tse and P.Viswanathan, *Fundamentals of Wireless Communication*. Cambridge University Press, 2005.

[17] C. Schlegel, *Waveform Communication*. ECED 3511 lecture notes, 2017.

[18] C. Schlegel , *AIF Quarterly Report*. 2017.

[19] S. Haykin and M. Moher, *Modern Wireless Communication*. Pearson-Prentice Hall, 2005.

[20] C. Schlegel and M. V. Burnashev, "The interplay between error control coding and iterative signal cancelation," *Trans. Sig. Proc.*, vol. 65, pp. 3020–3031, June 2017.

[21] C.Schlegel and D.Truhachev, "Multiple access demodulation in the lifted signal graph with spatial coupling," *IEEE Trans. Inform. Theory*, vol. 59, no. 4, pp. 2459–2470, 2013.

[22] D. Truhachev and C. Schlegel, "Coupling data transmission for multiple-access communications," *IEEE Trans. Inform. Theory., submitted, also arXiv:1209.5785*, June 2018.

[23] R. Dodd, C. Schlegel, and V. Gaudet, "Ds-cdma implementation with iterative multiple access interference cancellation," *Circuits and Systems I: Regular Papers, IEEE Transactions on*, vol. 60, pp. 222–231, 01 2013.

[24] M. Bashir, D. Truhachev, and C. Schlegel, "Kalman forward-backward channel tracking and combining for ofdm in underwater acoustic channels," in *2018 OCEANS-MTS/IEEE Kobe Techno-Oceans (OTO)*, pp. 1–10, IEEE, 2018.

[25] T.Kailath, S. Thomas, and B.Hassibi, "Linear estimation," *Prentice Hall*, 2000.

[26] P.Hoeher, "Stretched-exponential doppler spectra in underwater acoustic communication channels," *IEEE T. Vehicular Tech.*, vol. 41, no. 4, pp. 461–468, 1992.

[27] B.DVan Veen and K.M.Buckley, "Beamforming: a versatile approach to spatial filtering," *IEEE ASSP Mag.*, vol. 5, pp. 4–24, April 1988.

[28] C.Schlegel and M.Jar, “Embedded pilot and multi-size ofdm processing for jointly time and frequency selective channels,” *Intern. Symp. on Information Theory and Applications*, pp. 784–752, 2016.